Mapping hV4 and ventral occipital cortex: The venous eclipse

Jonathan Winawer
Department of Psychology, Stanford University, Stanford, CA, USA

Hiroshi Horiguchi
Department of Psychology, Stanford University, Stanford, CA, USA, & Department of Ophthalmology, Jikei University, School of Medicine, Tokyo, Japan

Rory A. Sayres
Department of Psychology, Stanford University, Stanford, CA, USA

Kaoru Amano
Department of Complexity Science and Engineering, University of Tokyo, Tokyo, Japan

Brian A. Wandell
Department of Psychology, Stanford University, Stanford, CA, USA

While the fourth human visual field map (hV4) has been studied for two decades, there remain uncertainties about its spatial organization. In analyzing fMRI measurements designed to resolve these issues, we discovered a significant problem that afflicts measurements from ventral occipital cortex, and particularly measurements near hV4. In most hemispheres the fMRI hV4 data are contaminated by artifacts from the transverse sinus (TS). We created a model of the TS artifact and showed that the model predicts the locations of anomalous fMRI responses to simple large-field on–off stimuli. In many subjects, and particularly the left hemisphere, the TS artifact masks fMRI responses specifically in the region of cortex that distinguishes the two main hV4 models. By selecting subjects with a TS displaced from the lateral edge of hV4, we were able to see around the vein. In these subjects, the visual field coverage extends to the lower meridian, or nearly so, consistent with a model in which hV4 is located on the ventral surface and responds to signals throughout the full contralateral hemifield.

Keywords: V4, receptive fields, occipital cortex, fMRI, functional imaging

Citation: Winawer, J., Horiguchi, H., Sayres, R. A., Amano, K., & Wandell, B. A. (2010). Mapping hV4 and ventral occipital cortex: The venous eclipse. *Journal of Vision, 10*(5):1, 1–22, http://journalofvision.org/content/10/5/1, doi:10.1167/10.5.1.

Introduction

There is a great deal of interest in how visual information is represented in human ventral occipital (VO) cortex. Much of the interest stems from functional magnetic resonance imaging (fMRI) reports of regions within VO that are responsive to highly specific stimuli such as colors, faces, words, scenes or objects (Cohen et al., 2000; Epstein & Kanwisher, 1998; Grill-Spector, Kushnir, Edelman, Itzchak, & Malach, 1998; Kanwisher, McDermott, & Chun, 1997; Lueck et al., 1989; Malach et al., 1995; Martin, Haxby, Lalonde, Wiggs, & Ungerleider, 1995). There also have been several measurements of visual field maps in regions that abut or overlap these stimulus-specific responses. Understanding the organization of stimulus-selective VO cortex with respect to VO maps promises to clarify a great deal about human object perception.

Progress in understanding the VO organization has been slowed because it is difficult to identify consistent visual field maps and stimulus-specific organization across observers. This experience stands in contrast to BOLD fMRI measurements of V1, V2 and V3; these maps can be measured easily and repeatably in nearly all subjects. In the experiments we report here, we set out to answer specific questions about one map that is located adjacent to V3 on the ventral surface—hV4 (Brewer, Liu, Wade, & Wandell, 2005; Hansen, Kay, & Gallant, 2007; McKeefry & Zeki, 1997; Wade, Brewer, Rieger, & Wandell, 2002; Wandell, Dumoulin, & Brewer, 2007). In trying to understand the difficulty in reliably measuring this map,

doi: 10.1167/10.5.1 Received September 11, 2009; published May 6, 2010 ISSN 1534-7362

we have come to appreciate some important limitations in measuring ventral occipital signals in general. In this report we describe both our specific conclusions about hV4 as well as our new understanding of limitations in measuring VO cortex.

Background: hV4

The location and responses of the fourth visual field map in human has a rich history (Brewer et al., 2005; Hansen et al., 2007; Lueck et al., 1989; McKeefry & Zeki, 1997; Tootell & Hadjikhani, 2001; Wade et al., 2002; Zeki et al., 1991). Here, we continue the story by considering a recent controversy concerning the visual field map coverage of this map in human (Brewer et al., 2005; Hansen et al., 2007; Larsson & Heeger, 2006; Wade et al., 2002).

In macaque, the V4 map spans the dorsal and ventral portions of the occipital lobe. In each hemisphere the map represents the contralateral hemifield; the dorsal portion of the map represents a little less than a quarter of the lower visual field. Since the first human measurements, however, investigators have not been able to reliably measure a dorsal component of V4 (Tootell & Hadjikhani, 2001). Moreover, the initial attempts to identify V4 based on functional color responses (McKeefry & Zeki, 1997; Zeki et al., 1991) and neurological case studies (Meadows, 1974) suggested that in human V4 is confined to the ventral surface. An exploration of the visual maps in these color responsive VO regions further suggested that the visual field coverage was significantly more than a quarterfield, and likely a hemifield. This too caused uncertainty about homology of the fourth human map with macaque V4. Hence, it was suggested that the fourth human map on the ventral surface be called hV4 (Wade et al., 2002).

Subsequent measurements have not produced definitive hV4 maps in every subject; the extent of the visual field coverage of the map on the ventral surface appears to vary between subjects. Some groups have assumed that the difficulty in measuring the full contralateral hemifield should be attributed to instrumental and methodological limits (Larsson & Heeger, 2006; Wade et al., 2002). Other investigators have proposed that the ventral hV4 field map does not extend to the lower vertical meridian (Hansen et al., 2007; Tootell, Tsao, & Vanduffel, 2003). They argue this coverage is missing in human and propose a model that adheres more closely to the macaque V4. Specifically Hansen et al. (2007) argue that a sliver of V4 is on the dorsal surface, and that this dorsal cortex contains a representation of the lower vertical meridian that is missing on the ventral surface. The two competing models are explained and contrasted in Figure 1.

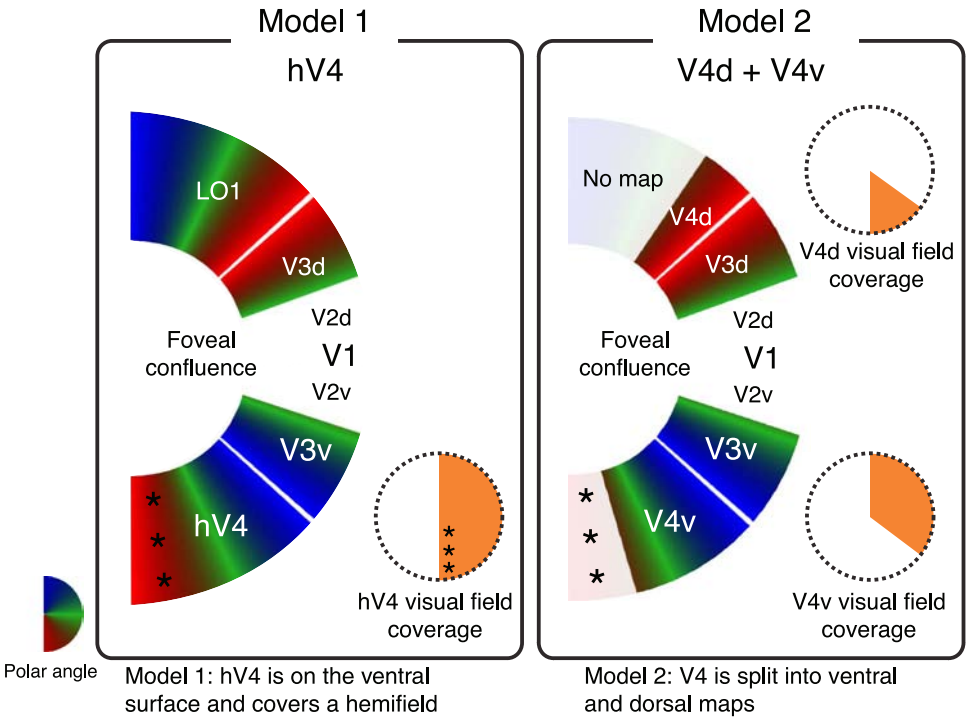

Figure 1. Two models of the organization of the visual field maps near the occipital pole. (1) In model 1, hV4 is entirely on the ventral surface, and responds to the complete contralateral hemifield (Brewer et al., 2005; Larsson & Heeger, 2006; Wade et al., 2002). (2) In model 2, V4 is split into a larger ventral region and a smaller dorsal region (Hansen et al., 2007). In this model, the ventral region is blind to the visual field near the lower vertical meridian. Asterisks, here and in other figures, indicate the lateral edge of hV4 according to model 1, with a putative lower field representation. According to model 2, there is no organized visual field map in this region.

We set out to examine the hV4 visual field map coverage on the ventral surface. As we began our measurements, we believed that the new population receptive field (pRF) techniques (Dumoulin & Wandell, 2008) coupled with additional specific measures of responses to stimuli on the lower vertical meridian, might be able to distinguish between the two models.

In pursuing these measurements, we discovered a limitation in our ability to measure the hV4 map in many hemispheres. Specifically, in most hemispheres the very large transverse sinus passes quite close to the hV4 map. We can now identify the position of this sinus both from anatomical scans and from its influence on functional measurements. We have discovered that in many cases, the effect of the transverse sinus is to mask the responses in the region of cortex that can decide between these models at the lateral hV4 boundary.

In Section Map organization of this report we describe the spatial organization and anatomical location of several visual fields maps near the occipital pole, including hV4. We show results from one subject in which the organization is particularly clear.

In Section Measurement limitations in ventral occipital cortex we describe the location and impact of the transverse sinus on BOLD measurements in VO cortex. We show that cortex near the sinus responds either unreliably or with misleading signals, masking the true neural response. Further, we show how to identify these regions from functional and anatomical measurements.

In Section hV4 measurements we return to the specific question that motivated this study: how far does the hV4 coverage extend? We use the biological variability of the position of the transverse sinus across the subject population to see around this large vein. We find that in subjects who have a transverse sinus that is displaced from hV4, functional responses extend to the lower vertical meridian, or nearly so, and the hV4 map covers the entire contralateral hemifield. In subjects where the TS runs near the lateral edge of hV4, the estimated coverage is sometimes substantially less than a hemifield. The most parsimonious interpretation is that the hV4 map covers the contralateral hemifield and that the apparently reduced coverage in many subjects is caused by the inability to measure cortex in the shadow of the TS artifact.

In the Discussion we show that the sinus, which runs through ventral occipital cortex, also limits measurements in other VO locations. These regions include other maps and object-selective regions, as well as the foveal representation at the posterior pole. The effect of the sinus cannot be eliminated by averaging across cortex or averaging across multiple sessions because the artifact does not simply add random, Gaussian noise. We discuss the implications of these observations for current attempts to understand the signals in ventral occipital cortex.

Methods

Subjects

Six subjects with normal or corrected-to-normal visual acuity participated in this study. All subjects participated in one scanning session to obtain a high resolution T1-weighted anatomical volume and 1–3 functional sessions to measure visual field maps. Informed written consent was obtained from all subjects.[1]

Stimulus presentation

Two display configurations were used for different sized stimuli. Large stimuli, spanning 14 deg of eccentricity, were presented on an LCD projector (NEC LT158) using optics that imaged the stimuli onto a back-projection screen in the bore of the magnet. The subjects viewed the display through a mirror. The viewing distance from the screen to the eye was 24–25 cm. Small stimuli, spanning 3 deg of eccentricity, were presented on an LCD flat panel display (NEC 2080UX) within a shielded box at the rear of the bore. The display was viewed through a mirror and the viewing distance was 180 cm.

Both the small and large displays were 800 × 600 pixels with a screen refresh rate of 60 Hz. All stimuli were restricted to a circular region within a 300-pixel radius of the center of the screen.

Visual stimuli were generated on a Macintosh MacBook Pro in the Matlab programming environment using custom software, made freely available (http://vistalab.stanford.edu/software/). The software tools are built on functions from the PsychToolbox (Brainard, 1997; Pelli, 1997).

During fMRI measurements subjects fixated on a small disc at the center of the screen (approximately 0.2 deg radius for large stimuli; approximately .06 deg radius for small stimuli). The subjects' task was to indicate with a key press each time the fixation disc changed color. The color alternated between red and green at random intervals unrelated to the stimulus sequence.

Large field on–off stimuli

For 4 subjects, simple on–off stimuli spanning the maximum visual field obtainable were presented in separate scans. These stimuli were presented in a circular aperture (14 deg radius). Within the aperture, a contrast pattern was presented for either 18 s or 12 s (ON periods), alternating with zero contrast mean-luminance periods for the same duration (OFF periods). Two subjects had 36-s periods five times per scan and two subjects had 24-s periods 6 times per scan. The contrast pattern comprised a moving dartboard. The checkerboard pattern within each

spoke of the dartboard (15 deg angle) moved in opposite directions, alternately inward and outward. The motion direction changed randomly (approximately every 2–3 seconds). Two to four large-field scans were obtained per subject.

The purpose of these scans was to assess the reliability of visually driven BOLD signals, particularly with regard to regions of VO cortex thought to be influenced by TS artifacts. Visually responsive neurons (other than those with very peripheral receptive fields) are expected to respond in phase with the contrast pattern. Failure to observe such responses in a region of visual cortex indicates that the region cannot be accurately mapped.

Lower meridian on–off stimuli

For 5 subjects, on–off stimuli confined to a wedge along the lower meridian were presented in a separate scan session. These stimuli were identical to the large-field on–off stimuli, except that the aperture was limited to a wedge spanning the lower vertical meridian, extending either 22.5°, 45°, or 90° bilaterally from the lower meridian. The contrast pattern was presented within the aperture for 18 s (ON periods), alternating with 18 s of mean luminance (OFF periods), with 6 cycles per scan. Each of the three stimulus sizes was presented in a separate scan, and each scan was repeated 2–3 times in pseudorandom order.

The purpose of these scans was to supplement the visual field mapping experiments by providing an independent measurement of the response in hV4 to stimuli presented along the lower vertical meridian.

Visual field mapping stimuli

The mapping stimuli were slowly moving rectangular bars, described in more detail in previous work (Amano, Wandell, & Dumoulin, 2009; Dumoulin & Wandell, 2008). The stimuli are briefly described here. The bar positions were displaced in discrete steps in synchrony with the fMRI volume acquisition, i.e. every 1.5 seconds. The bars contained high contrast checkerboards that drifted within the bar aperture. Four bar orientations (0, 45, 90 and 135 deg from vertical) and two different motion directions were used, giving a total of 8 different bar configurations within a given scan for 192 seconds.

Four blank periods (zero contrast) were interleaved in each scan for 12 s each. Each of these blank periods replaced a different position of the bar stimulus. The blank periods are important for estimating large pRF sizes (Dumoulin & Wandell, 2008).

Large and small mapping stimuli were presented in separate scan sessions (5–10 scans each), except for one subject for whom all scans were obtained in a single session (4 large-bar scans, 2 large-field on–off scans, and 2 small-bar scans).

Pilot scan sessions also included mapping stimuli with rotating wedge apertures and expanding ring apertures. Models fit with all three stimulus types (bars, wedges, rings) yielded similar data to those obtained with bars alone. Since it was more efficient to scan with bars alone, wedge scans and ring scans were discontinued. All mapping results presented are for bar scans only.

MR acquisition

Anatomical data

T1-weighted anatomical images were acquired on a 1.5 T Sigma LX scanner with a vendor-supplied head-coil using a 3D-SPGR pulse sequence (1 echo, minimum TE, flip angle 15 deg, effective voxel size of 0.94 × 0.94 × 1.2 mm^3). We acquired at least 2 whole brain T1-weighted anatomical MRI data sets for each subject. These data were averaged and re-sampled to isotropic resolution at either 1 mm^3 (3 subjects), 0.8 mm^3 (1 subject), or 0.7 mm^3 (2 subjects). A surface-coil anatomical MRI, taken at the same time as the functional images, was aligned with the head-coil anatomical MRI using two automated alignment algorithms, a robust multi-resolution algorithm (Nestares & Heeger, 2000), and an algorithm that maximizes mutual information (Ashburner & Friston, 2003; Maes, Collignon, Vandermeulen, Marchal, & Suetens, 1997). The functional images and surface-coil anatomical data acquired in the same session were co-registered. Using the spiral acquisition and small field of view surface-coil limits the spatial distortions between the functional and surface-coil anatomical images. Hence, we used the transformation derived from the surface-coil anatomicals to align the functional data to the head-coil anatomicals.

White matter was segmented from the head-coil anatomical MRI using custom software (itk-Gray, http://white.stanford.edu/software/), modified from ITK-SNAP http://www.itksnap.org; (Yushkevich et al., 2006) and hand-edited to minimize segmentation errors (Teo, Sapiro, & Wandell, 1997). Gray matter was grown from the segmented white matter to form a 3 mm layer covering the white matter surface. The cortical surface was represented as a mesh at the white/gray matter border. This mesh was used to render a smoothed 3D cortical surface or to flatten the cortical representation (Wandell, Chial, & Backus, 2000). In the smoothed 3D representations dark regions indicate sulci and light regions indicate gyri.

Venogram

The dural sinuses can be identified on a standard high resolution T1 anatomical image by their low luminance value and anatomical location. To precisely label the sinuses, we made 3D phase contrast measurements using gradient echo (TR 19 ms, TE 6.8 ms, flip angle 15°, velocity encoding 40 cm/s). Slices were oriented sagitally, 1.5 mm thick with no interslice spacing, and 0.93 × 0.93 mm

inplane resolution. A T1-weighted anatomical scan was acquired in the same session, and used to align the venogram with the stored, high-resolution T1. The dural sinuses were labeled from the venogram using the flood-fill tool in itk-Gray.

Functional data

Functional magnetic resonance images were acquired with a 3T General Electric Sigma scanner and a receive-only quadrature surface coil (Nova Medical, Wilmington, MA) centered over the subject's occipital pole. The effective voxel size was 2.5 mm isotropic (FOV = 22.0 × 22.0 cm^2). Functional MR images (TR/TE 1500/30 ms, flip angle 71 deg) were acquired using a self-navigated spiral-trajectory pulse sequence (Glover, 1999; Glover & Lai, 1998). 20 slices with no gap between them were acquired, oriented approximately perpendicular to the calcarine sulcus. The slice prescription included all of occipital cortex, as well as posterior parietal and temporal cortex.

MR analysis

Pre-processing

We analyzed fMRI data using custom software (http://vistalab.stanford.edu/software/). Data in each fMRI session were analyzed voxel-by-voxel with no spatial smoothing. The raw data were pre-processed in several steps. Data were slice-time corrected to compensate for the difference in the time of acquisition across slices within each 1.5-s frame. Head movements across scans were examined by comparing the mean value maps of the BOLD signals, and motion correction algorithm was applied; most scans had minimal head motion (less than one voxel). Motion artifacts within each scan were also corrected. These were typically very small (less than 0.5 voxels). No scans had significant motion artifacts. The motion- and slice-time-corrected time series from all scans with the same stimulus were then averaged. Thus for each subject, one average time series was generated from the small-stimulus bar scans, one from the large stimulus bar scans, one from the large-field, on–off scans (four subjects), and one for each of three lower wedge on–off scans (five subjects). From these averaged time series, the BOLD signal from each voxel was divided by its mean to derive a time series of percentage modulation. Baseline drifts were deducted from the time series by high-pass temporal filtering. Filtering and transformation to percentage modulation were omitted for computation of mean maps.

Mean BOLD maps

Mean BOLD maps were derived for each subject from each of the averaged scans. The mean map was computed by taking the average value from the time series across the complete scan, using the pre-processed data (slice-time corrected, motion-corrected, and averaged across all scans with the same stimulus) without temporal filtering or converting to percentage modulation. The mean map was then normalized by dividing the value for each voxel within a hemisphere by the highest value within that hemisphere. Thus the normalized mean maps range from 0 to 1. The mean maps were then transformed to the high-resolution T1-weighted anatomy using trilinear interpolation (see section Anatomical data). The mean maps for a given subject were highly correlated across scan sessions. We therefore averaged the mean maps from the small-stimulus bar scans and the large-stimulus bar-scans to derive a single mean map for each subject. Note that the mean map is effectively unrelated to the stimulus: stimulus-related activity tends to cause modulations on the order of 1%, whereas factors like tissue type, distance from the imaging coil, and scanner artifacts can cause signal variations on the order of 5-fold.

Coherence analysis for on–off scans

The on–off stimuli were presented as a temporal square wave in a block design (Large field on–off scans: 18 s on–18 s off, 5 cycles, or 12 s on–12 s off, 6 cycles; lower wedge scans: 18 s on–18 s off, 6 cycles). The convolution of a square wave at these time scales and the hemodynamic response is approximately a harmonic, so the data were analyzed using a coherency analysis. The coherence was calculated as the ratio of the power at the stimulus frequency (5 cycles per scan or 6 cycles per scan) to the sum of the powers at all other frequencies. The coherence at the stimulus phase was calculated by multiplying the calculated coherence by the cosine of the difference in phase between the stimulus (after compensating for the hemodynamic lag) and the response. This measure yields positive values for responses near the stimulus phase and negative values for responses in counterphase to the stimulus. Color overlays in figures showing responses to on–off stimuli include only those voxels whose coherence exceeded 20%.

PRF analysis

We used a model-based method to estimate visual field maps and population receptive fields (pRF) (Dumoulin & Wandell, 2008). The pRF is defined as the region of visual space that stimulates the recording site (Dumoulin & Wandell, 2008; Jancke, Erlhagen, Schoner, & Dinse, 2004; Victor, Purpura, Katz, & Mao, 1994). Details of the pRF analysis are described in a previous study (Dumoulin & Wandell, 2008). Briefly, for each voxel we predicted the BOLD response using a 2D Gaussian pRF model; the parameters are center location (x, y) and spread (s), the standard deviation of the Gaussian. All

parameters are expressed in degrees of visual angle. The predicted fMRI time-series is calculated by a convolution of the model pRF with the stimulus sequence and then an additional convolution with the BOLD hemodynamic response function (HRF) (Boynton, Engel, Glover, & Heeger, 1996; Friston et al., 1998; Worsley et al., 2002); the pRF parameters for each voxel minimize the sum of squared errors between the predicted and observed fMRI time-series. Angle (atan(y/x)) and eccentricity (sqrt($x^2 + y^2$)) are derived from the center location parameters (x, y).

The pRF model was computed on the segmented gray matter in the T1-weighted anatomy after transforming the time series by trilinear interpolation. This is in contrast to the mean maps and coherence maps, which were computed at the resolution of the acquired functional data and then transformed to the T1-weighted anatomy. The reason for calculating the pRF model on the transformed time series is that the first stage of the pRF analysis, the coarse grid fit, operates on data that are spatially smoothed along the cortical surface, requiring a mesh representation (Dumoulin & Wandell, 2008). The second stage, the search fit, operates on unsmoothed data.

Composite pRF models

For each subject, separate models were fit to the small- and large-stimulus bar scans. Inspection of the models showed that foveal representations in visual cortex were better fit by the small-stimulus models while more peripheral regions were better fit by the large-stimulus models. To visualize maps that spanned the fovea and periphery, we derived a composite model for each subject. The composite model was created by a simple minimization rule: For each voxel, the composite model drew all the pRF parameters (x, y, s) from the single-stimulus model with a lower sum of squared error (or, conversely, greater variance explained) between the predicted and observed fMRI time series. For all analyses with pRF model parameters (visual field maps, visual field coverage plots, and pRF size versus eccentricity plots), voxels were included only if the variance in the time series explained by the pRF model exceeded 15%. PRF model parameters for all analyses and plots come from the composite model, except for analysis of receptive field size as a function of eccentricity, which uses model parameters fit to the large-stimulus scans only.

Visual field coverage

Visual field coverage was estimated according to the methods described by Amano et al. (2009), with a few minor differences. Visual field coverage defines the locations within the visual field that evoke a significant response from voxels within a map. We estimate the visual field coverage from the full pRF. We first identify the pRF centers across all of the voxels within a visual field map. For each subject, we create a binary image showing whether a pRF center exists at each visual field location. We then estimate the visual field coverage by combining the pRF center and size estimates. Specifically, from each voxel we estimate the 2D Gaussian in the visual field (stimulus-referred). Many points in the visual field are covered by at least one pRF, and we create a map that represents the highest pRF value at each visual field location. To reduce the effect of outliers, we bootstrap over 100 repetitions. We randomly sample with replacement from all pRFs within a region of interest to generate one coverage map. This is repeated 100 times to make 100 coverage maps, and the mean of these maps is taken as the coverage map for a region of interest. Because the peak value of the 2D Gaussian model is normalized to 1, the range of values in each subject's map is between 0 and 1. We created these maps for each subject, and superimposed the center map (gray dots) on the coverage map (hot colors). Because a single voxel with a very large receptive field can give a high value to the entire visual field, one anomalous voxel can have a great effect on the coverage map. To minimize the effect of anomalously large receptive field size estimates, we smoothed the pRF size parameter (s) with a median filter: for each voxel in a map, we found the two nearest neighbors in stimulus space (the two voxels with the closest pRF centers), and replaced that voxel's size parameter with the median of the three voxels' sizes.

Results

Map organization

Many of the occipital visual field maps can be seen in a single view from the posterior occipital pole (Figure 2). The polar angle maps measured using the composite pRF model clearly show the boundaries of eleven maps. The view is adjusted so that hV4, located on the ventral–lateral portion of the occipital pole, is centered in the image. It is possible to measure many of these maps in many subjects, but in different subjects there are often imperfections in the measurements that obscure one or more features.

Posterior maps—V1, V2, V3

The general organization of the posterior-medial maps is well agreed upon. Primary visual cortex, V1, straddles the calcarine sulcus. The polar angle representation stretches from the lower meridian (red) to the upper meridian (blue), spanning the upper and lower banks of the calcarine sulcus, respectively. V2 is shaped like a U surrounding V1 (Schira, Tyler, Breakspear, & Spehar, 2009). The ventral and dorsal portions of V2 abut V1 on either side. These boundaries are identified by polar angle

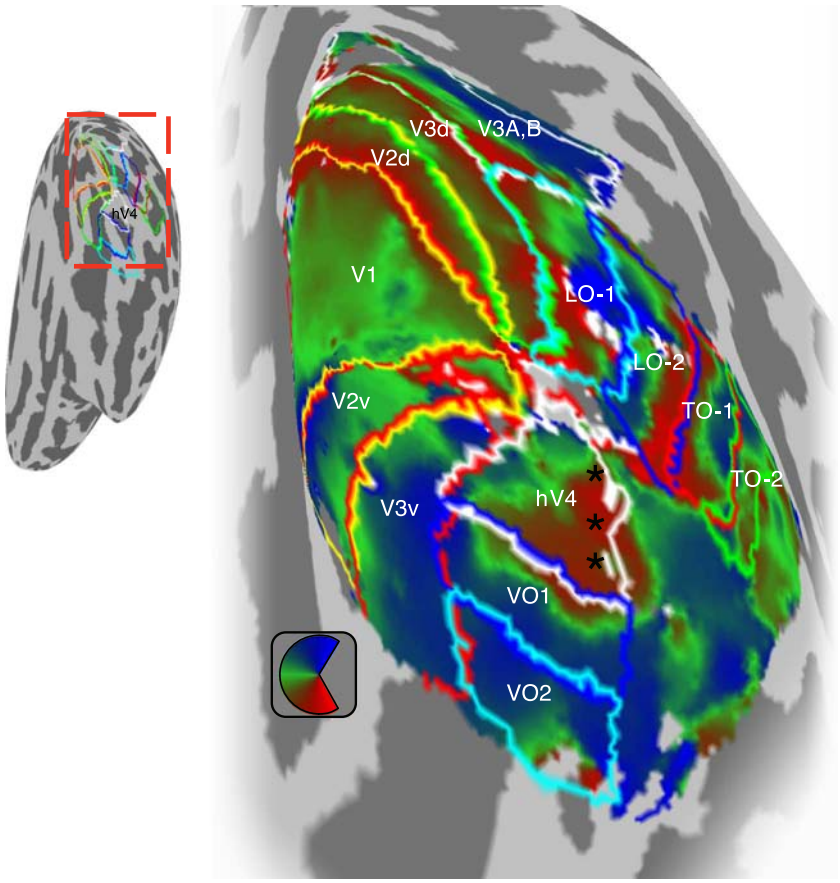

Figure 2. Organization of the visual field maps near the occipital pole. In this subject (S1) hV4 on the ventral surface and LO-1 on the dorsal surface are consistent with model 1 (Figure 1). The asterisks denote the lateral edge of hV4. The inset at the upper left shows the magnified region of the main image. The color inset shows the angle representation. Other maps: VO-1,2 (Brewer et al., 2005), ventral/anterior to hV4; LO-2 (Larsson & Heeger, 2006), TO-1,2 (Amano et al., 2009) adjacent and anterior to LO-2; and V3A,B (DeYoe et al., 1996; Press, Brewer, Dougherty, Wade, & Wandell, 2001; Tootell et al., 1997) superior to V3d and LO-1.

reversals near the upper and lower vertical meridians, respectively. V3 is also shaped like a U surrounding V2. The V2/V3 boundaries are identified by horizontal polar angle reversals (green).

Ventral maps—hV4, VO-1,2

On the ventral occipital surface, hV4 borders a section of V3v (blue). The boundary is identified by an upper-field polar angle reversal. Continuing laterally, the polar angle representation in hV4 transitions to horizontal (green) and lower (red). The lateral edge of hV4 is marked by asterisks to highlight the critical region identified in the Figure 1 models. The lower field representation in this figure is consistent with the hemifield model.

hV4 does not extend as far anterior as V3; rather, hV4 curves so that the lower visual field representation on its lateral edge extends dorsally/medially toward V3v. This lower field representation forms the posterior edge of VO-1 (Brewer et al., 2005). That map continues anteriorly until the upper field reversal, marking the boundary with VO-2.

Dorsal maps—V3A,B, LO-1,2, TO-1,2

The dorsal/lateral edge of V3d is marked by a lower-field polar angle representation. This lower-field boundary along V3 is shared with two other field maps. The anterior portion of this boundary is shared with V3A. The posterior portion of this boundary is shared with LO-1. The LO-1 map spans an approximate hemifield, from the lower field edge shared with V3d to the upper field edge shared with LO-2. The data in this subject are consistent with the LO-1,2 model proposed by Larsson and Heeger (2006) and since replicated by Amano et al. (2009). It is thus inconsistent with the split model of V4 (Figure 1; (Hansen et al., 2007)), which predicts a narrow lower field representation at the V3d/V4d border adjacent to a non-retinotopic, object-selective region. Hence the presence of a hemifield LO-1 map adjacent to V3d indirectly supports the hemifield model of hV4. Anterior to LO-2 are two more hemifield maps, recently described by Amano et al. (2009), who refer to them as TO-1,2, for their temporal occipital locations. These maps probably correspond to MT and MSTl as measured in macaque.

No man's land

Note the large unmarked region between the dorsal maps (LO-1,2, TO-1,2) and the ventral maps (hV4, VO-1,2). This region is not well understood. The posterior part of this region may be part of the confluent fovea at the center of the pinwheel containing V1, V2, V3, LO-1,2, and hV4. The more anterior part of this region may include object-selective regions such as the lateral occipital complex (Malach et al., 1995) or visual word form area (Ben-Shachar, Dougherty, & Wandell, 2007; Cohen et al., 2000). The retinotopic maps that otherwise tile the occipital lobe are often missing in this region. The polar angle representations that we do observe in this region, as in Figure 2, differ substantially across subjects. To anticipate the results in the next section, we note that in most subjects this region is adjacent to the TS.

Measurement limitations in ventral occipital cortex

The transverse sinus distorts the local magnetic field

The visual field maps in Figure 2 are clear, but this is not the case in every subject; the variance across subjects is particularly strong in ventral occipital cortex. To interpret the BOLD signal in this region requires understanding the source of this variance. One likely source can be traced to the dural sinuses, a set of large vessels that collect venous blood from the interior and exterior veins of the brain and drain into the jugular veins. Several of the dural sinuses, the transverse sinuses, the straight sinus, and the superior sagittal sinus, combine near the occipital pole (Figure 3a). The transverse sinus follows a path between the ventral occipital lobe and the cerebellum,

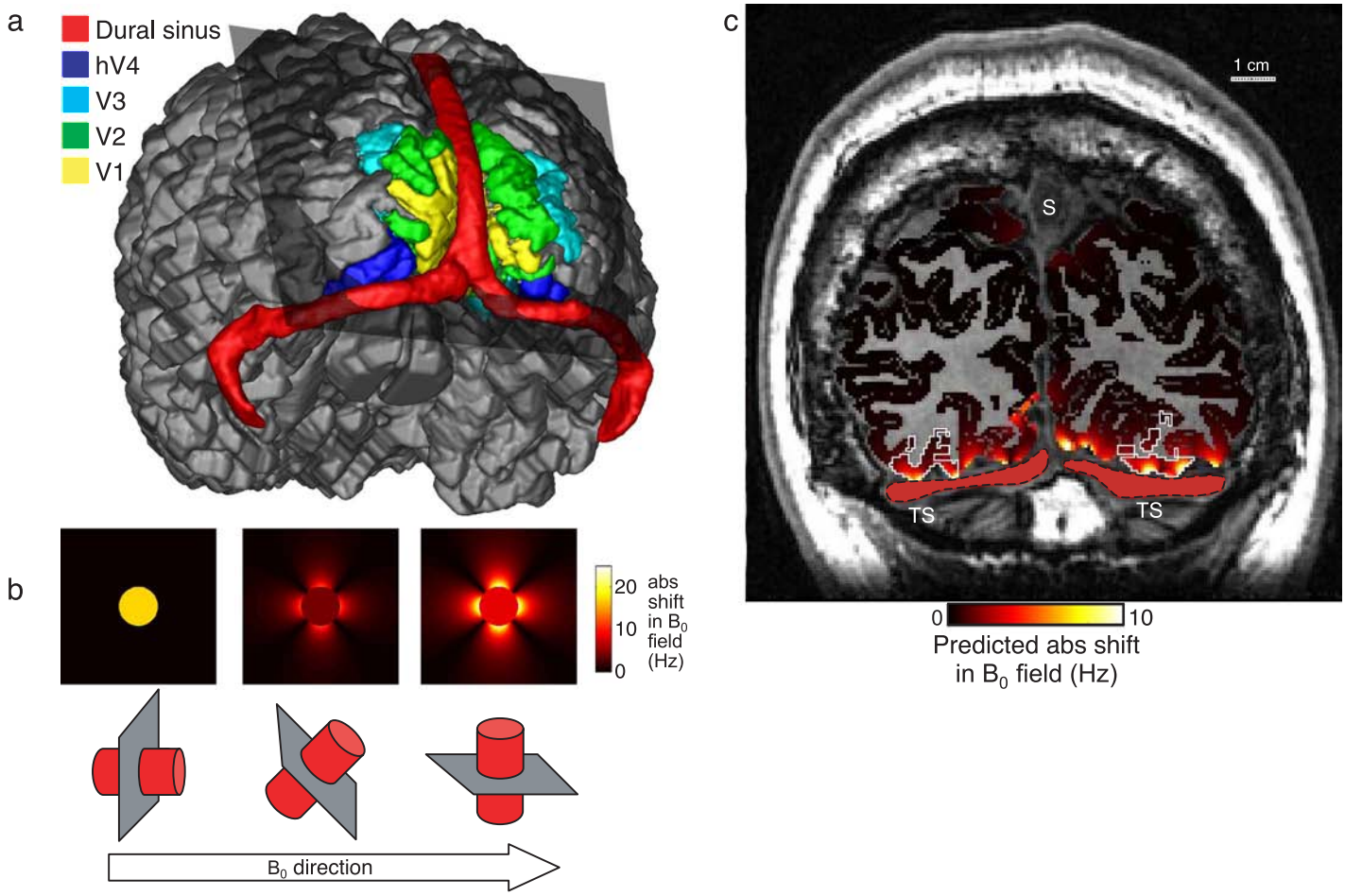

Figure 3. Location of transverse sinus and its effect on the mean magnetic field (B_0). (a) Position of the transverse sinus (red) with respect to the cortical surface and several visual field maps. (b) Simulation of the shift in B_0 caused by a cylinder containing venous blood. The size of the B_0 shift depends on the orientation of the cylinder with respect to the magnetic field. A local change in the B_0 field produces a change in the Larmor frequency, hence the shift is expressed in units of Hz (see color overlay; after Jezzard & Ramsey, 2003). (c) Cross-sectional view of the predicted shift in the B_0 field within the gray matter in a single image plane (indicated in (a)). The B_0 field is oriented approximately vertically in the plane. The white outlines show the estimated position of hV4. The TS is shaded red and outlined by black dashed lines. The position of the superior sagittal sinus is marked (S) at the dorsal midline. The size of the predicted B_0 shift is shown by the color overlay. In this subject, the predicted shift is large in both right and left hV4. The method used for predicting the B_0 shift is described in Appendix A. Subject S6.

usually within a few millimeters of the hV4 maps. The sinuses are visible on a T1-weighted anatomical scan.

The dural sinuses introduce significant B_0 inhomogeneities in nearby ventral cortex. The size of the B_0 shift in the proximity of a cylindrical vascular segment, such as the large dural sinus, depends on a number of factors. One is the cylinder diameter (6–8 mm) and another is the orientation of the cylinder with respect to the B_0 field (Ogawa, Lee, Nayak, & Glynn, 1990; Jezzard & Ramsey, 2003, Figure 3b). In general, the sinus influences signals on the gyri more than sulci simply because gyri are closer.

When a subject is lying supine in a scanner, the transverse sinus is positioned approximately orthogonal to the B_0 direction, making hV4 especially vulnerable to BOLD artifacts. We can calculate the expected size of the B_0 shift in hV4 (Figure 3c). In this coronal image, the transverse sinus is highlighted in red, and the superior sagittal sinus is easily visible as the labeled (S) dark region. The overlaid color maps shows how much the B_0 shift in VO cortex changes the Larmor frequency near the sinuses. Because the effective Larmor frequency in these regions differs from the frequency used during imaging, the reconstructed image is subject to distortions.

Functional signals near the transverse sinus fail to measure local cortical activity

It is often possible to use functional data to identify cortical locations where the TS shifts the B_0 value. The left image in Figure 4 shows that the shadow of the sinus is visible in the mean BOLD signal from a spiral k-space acquisition. Comparing the left and middle images shows that the locations with low mean BOLD signal correspond well with the locations with the largest predicted shift in the B_0 field. The low mean BOLD signal in the anterior temporal lobe arises from a different source: the susceptibility artifact caused by the ear canals.

The right image shows that responses near the TS artifact to large-field on–off modulations fail to accurately measure the cortical signal. We expect neurons to respond more to a moving contrast pattern (on) than to a uniform field (off). The BOLD responses throughout most of visual cortex are in-phase with the on–off stimulation (hot colors). However, in regions near the TS artifact, voxels generally respond in the opposite phase (blue). The locations where the B_0 field shift is high contain out-of-phase responses. This observation is confirmed in plots that show the full distribution of response phases as a function of the predicted shift in the B_0 field (Appendix B). Given that responses to on–off

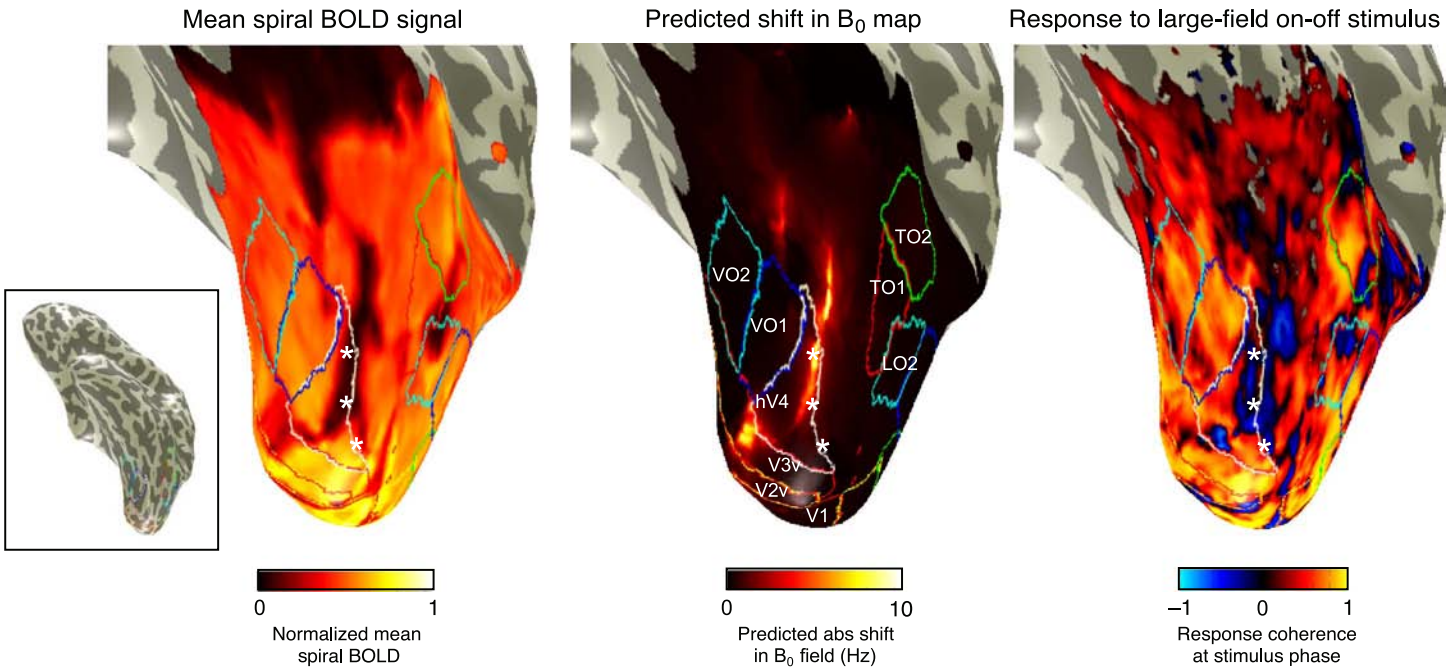

Figure 4. fMRI responses from locations with shifted B_0 values fail to accurately record local cortical activity. The three main images show the left ventral occipital cortex in S6. The colored outlines identify several visual field maps, and the asterisks mark the lateral edge of the hV4 map. The color overlay in the middle image measures the predicted shift of the Larmor frequency caused by the TS. The overlay in the left image measures the mean BOLD signal. The right image overlay shows the response coherence at the stimulus phase during large-field on–off scans. Responses in-phase with the stimulus have positive values (hot colors); responses in counterphase to the stimulus have negative values (cool colors). The locations with large predicted shifts in the Larmor frequency also show counterphase responses to the large-field on–off stimulus. The position of the TS artifact is well aligned with the estimated lateral edge of hV4. For this subject the BOLD responses in this location do not accurately record cortical activity.

contrast modulations fail to measure the cortical signal, it is quite likely that the responses to traveling wave or moving bar stimuli used for visual field mapping also fail.

The phase-reversed responses in the TS artifact region do not appear to depend on the precise parameters used in acquiring the MR images; for the subject shown in Figure 4, a large-field on–off scan acquired with a different scanner (Siemens versus GE), a different slice prescription (sagittal versus oblique), a different pulse sequence (EPI versus Spiral), and a different stimulus duty cycle (12.5% versus 50%) resulted in a highly similar pattern of responses, with out-of-phase responses observed in the same regions (data not shown).

The nature of the measurements near the TS artifact varies across conditions. In some cases, we find that the BOLD signal is unreliable across scans, in the sense that the same stimulus does not produce the same response. In many other cases, we find the signal to be reliable but wrong, as in the counterphase responses of Figure 4.

The TS artifact probably differs from another type of artifact caused by the large draining veins that pass through the cortical voxels. The changing oxygen content in these veins introduces a large modulation of the BOLD signal. This modulation can be an order of magnitude greater that induced by neural metabolism. The artifacts from some, but not all, veins embedded within cortex voxels can be identified by the very high variance of the BOLD signal in these voxels (Dagli, Ingeholm, & Haxby, 1999; Lee, Glover, & Meyer, 1995; Menon, 2002; Olman, Inati, & Heeger, 2007).

Because the TS artifact mechanism likely differs from the draining veins artifact, the BOLD signature of the TS artifact differs too. Responses within the TS artifact region are similar in modulation amplitude and reliability to responses in nearby cortex. We have identified the incorrect BOLD modulation near the TS because we know visual cortex responds synchronously to on–off modulations. Without such knowledge, one might simply accept the signals near the TS as legitimate measures of cortical activity.

Potential methods for avoiding the artifact

Within subjects, the TS artifact cannot be eliminated by averaging the BOLD signal; the TS artifact is more pernicious than adding random, zero-mean noise. For example the data in Figure 4 (right) represent the average of several scans. The regions in the TS artifact area that respond out of phase to the stimulus do so in each individual scan. Moreover the distribution of phases

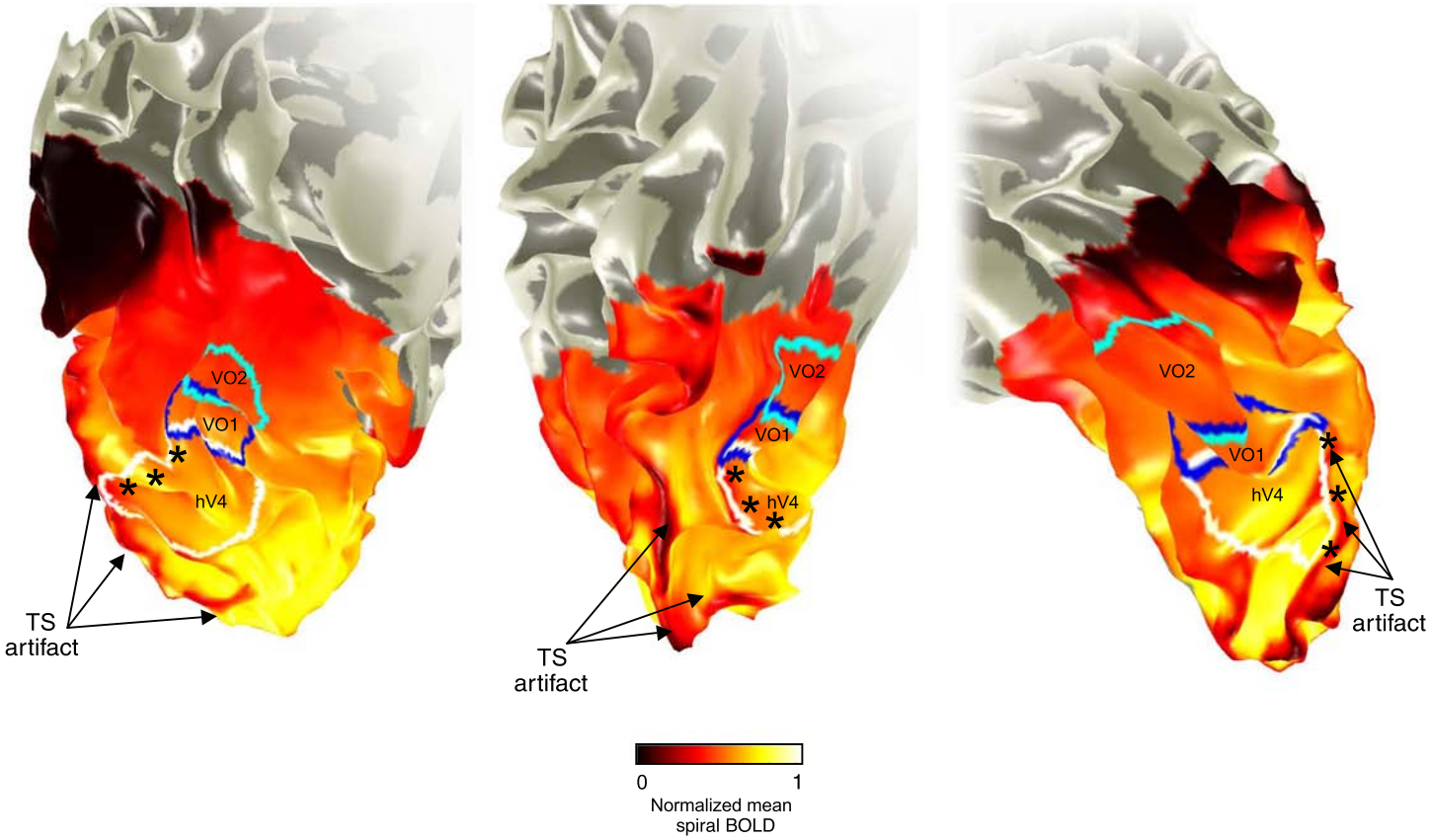

Figure 5. The location of the TS artifact relative to hV4 in three hemispheres. The two hemispheres (S3, S4, right hemispheres) on the left show a TS artifact (black arrows) that is largely displaced from the lateral edge of hV4 (asterisks). The hemisphere on the right side is an example in which the TS artifact runs along the length of the lateral edge of hV4 (S5, left hemisphere).

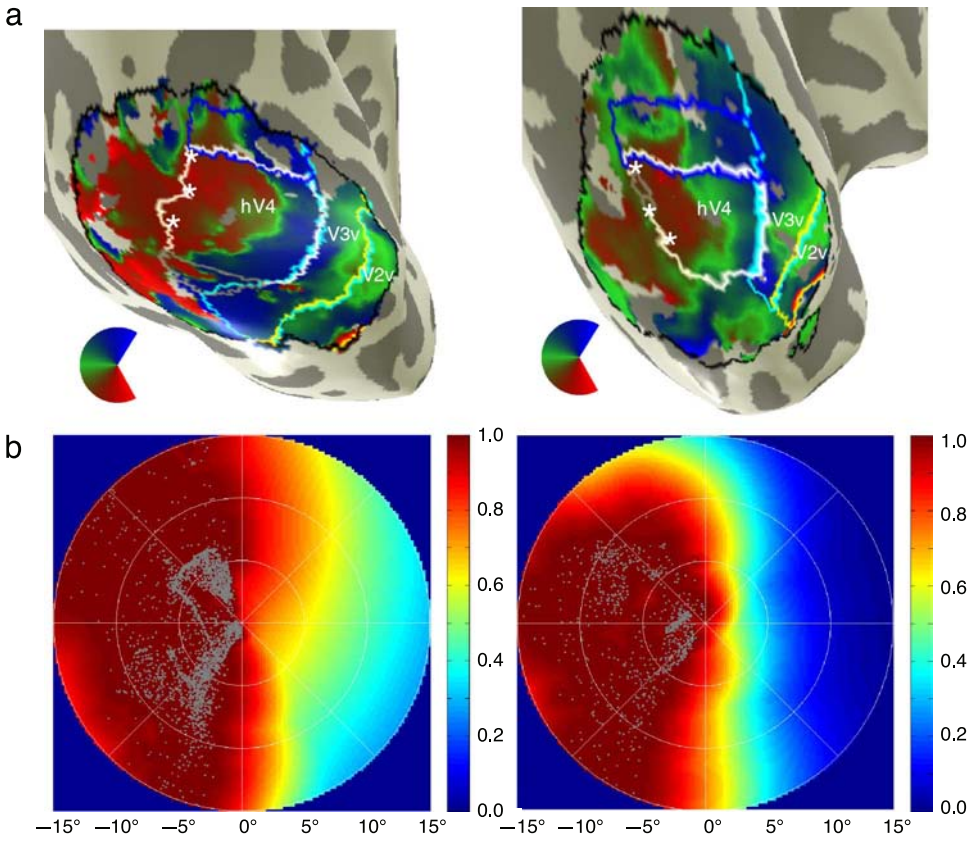

Figure 6. Visual field coverage in hemispheres with the TS displaced from the lateral edge of hV4. In these two subjects (S3, S4, right hemispheres) the pRF centers approach the lower vertical meridian and the coverage extends beyond the meridian. (a) Angle maps from the composite pRF models (14° and 3°). The gray outline marks the relatively small regions of hV4 that are affected by the TS artifact. (b) Visual field coverage. The image represents the central visual field (15 deg radius). The gray dots indicate the center of the pRF for each hV4 voxel. The color overlay represents the relative effectiveness of visual field locations at evoking a response in hV4.

across voxels in the artifact region is not random (Appendix B). Hence averaging the data cannot eliminate the artifactual responses. Across subjects averaging is no help because the TS is generally located in the same position, and its effect is greater in gyri than sulci. Thus, the methods used for measuring statistic parameter maps do not eliminate the artifact.

There is one piece of bright news among this generally gloomy assessment. It should be possible to find an instrumental solution to the TS artifact. The TS distorts the mean magnetic field (B_0); obtaining accurate estimates of this distortion might enable us to correct for the distortion during the reconstruction process.

hV4 measurements

Hemispheres in which the TS is displaced from hV4 support the hemifield model

While the TS often obscures responses from the lateral edge of hV4, there is some biological variability in the TS position. Specifically, in some hemispheres the TS can be more than 1 cm away from the lateral edge of hV4 which offers a chance of measuring responses from the full extent of this field map. Three hemispheres showing the different locations of the TS are shown in Figure 5. For the two hemispheres on the left of the image, the low mean BOLD signal is located posterior and lateral to the hV4 border. For the hemisphere in the right of the image, the TS artifact aligns with the lateral edge of hV4. We show the visual field maps from these three subjects in Figures 6 and 9.

In the hemispheres with the TS displaced from the lateral edge of hV4, the lateral edge of hV4 responds principally to stimuli located on the lower vertical meridian (Figure 6a), consistent with the hemifield model of Figure 1. In both of these hemispheres the distribution of pRF centers in hV4 extends close to the lower vertical meridian (Figure 6b, gray dots), though they do not extend into a small sliver of the field near the lower vertical meridian representation (about 10 deg, Figure 6b-left; and 20 deg, Figure 6b-right). But when the pRF size is taken into account, we find that hV4 responds to stimuli up to and beyond the vertical meridian.

It is important to combine pRF size and center location in estimating a map's visual field coverage. Accounting for

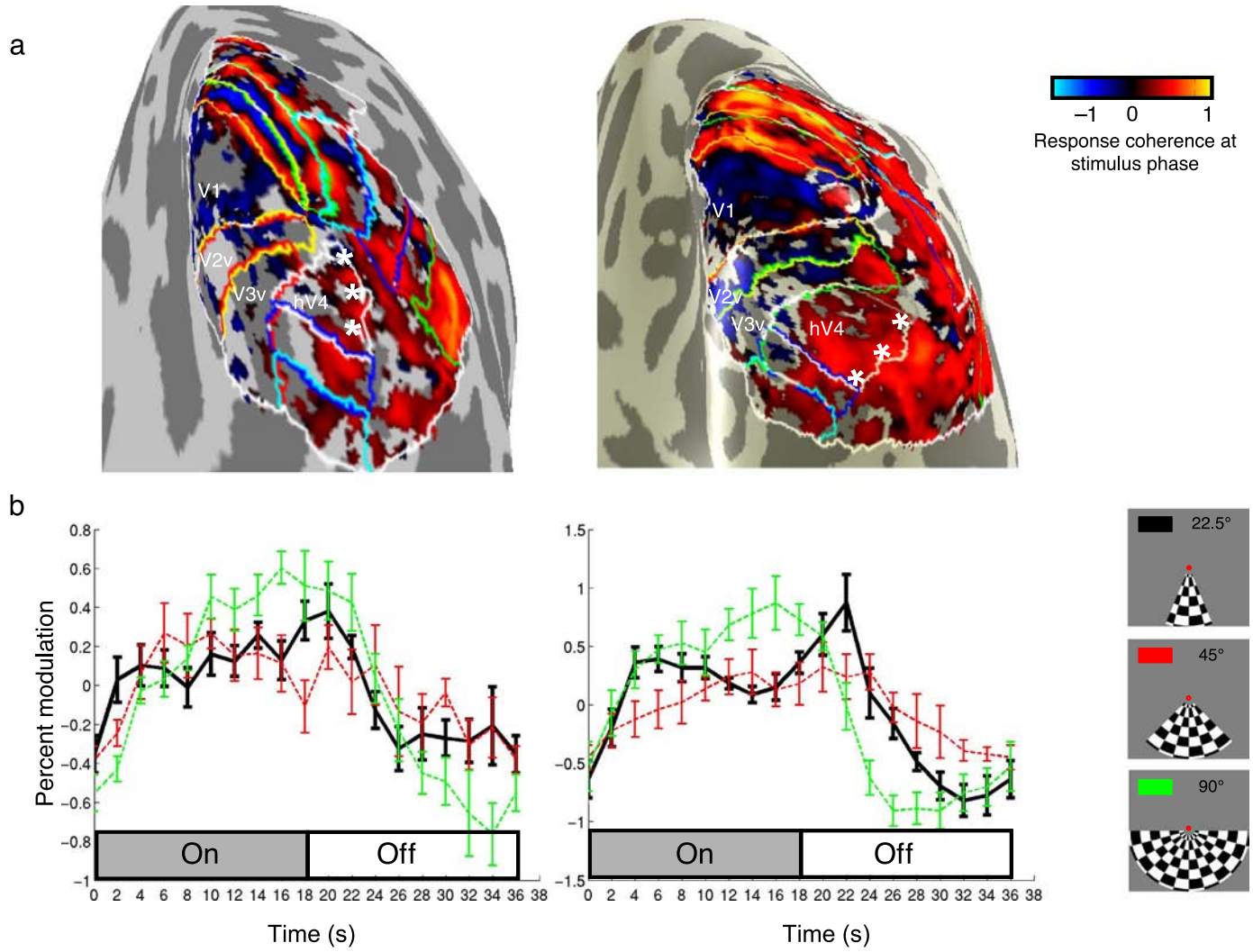

Figure 7. HV4 responds to stimuli near the lower vertical meridian. (a) The posterior view shows the spatial pattern of response coherence as the stimulus alternates between a lower vertical meridian contrast pattern (22.5 deg angular extent) and a uniform field. Responses in-phase with the stimulus have positive values (hot colors); responses in counterphase to the stimulus have negative values (cool colors). There are significant positive responses in hV4, but very little response or weak negative responses in ventral V1, V2 and V3. (b) We defined a region of interest along the lateral edge of hV4, extending 4 mm on either side. The fMRI time series in this ROI modulates significantly as the stimulus alternates between a contrast pattern near the lower vertical meridian and a uniform field. Across scans we used contrast patterns with different angular extents (inset at right), but the response modulation remained similar. This suggests that the stimulus near the lower vertical meridian is the most effective portion. Note that the time series represents the mean data from all voxels in the ROI; data are not thresholded by coherence (S1, left; S3, right).

the pRF center alone biases coverage estimates away from the vertical meridians. The vertical meridian represents an extreme boundary in the range of angular representations. Hence, any pooling of signals will move the estimate away from the boundary towards the center of the distribution. The pooling can occur because of fMRI voxel size and blurring. Bias away from the vertical midline can also arise because of neural circuitry. For example, if receptive fields of individual neurons in an early processing stage (such as V1) are largely limited to the contralateral visual field, then downstream neurons (e.g., in hV4) summing many such inputs will have receptive field centers skewed away from the vertical. (See Larsson & Heeger, 2006, p. 13137, for a more detailed discussion.)

hV4 responds to lower vertical meridian stimuli

The visual field coverage estimates show that hV4 responds significantly to stimuli on the lower vertical meridian. We independently evaluated this estimate by measuring the fMRI responses near the lateral edge of the hV4 field map to contrast stimuli that span the lower vertical meridian symmetrically (Figure 7). The responses in two subjects with relatively complete hemifield visual

field coverage show that hV4 responds to patterns restricted to within 22.5 deg (angular) of the lower vertical meridian.

For comparison, note that there are no responses, or only weak phase-reversed responses, to lower vertical meridian stimuli in ventral V1, V2 and V3.

We further measured the responses at the lateral edge of hV4 to stimuli spanning 90 and 45 deg around the lower vertical meridian. The responses to these stimuli do not differ significantly from the response to the 22.5 deg stimulus. This suggests that the principal signal driving the response at the hV4 lateral edge arises from the portion of the stimulus at the lower vertical meridian.

The hemispheres illustrated in Figures 6 and 7 are all right hemispheres. In most of the left hemispheres the TS artifact masks the critical hV4 region where measurements can distinguish between the two visual field map models (Appendix C). In many of the right hemispheres hV4 responds to stimuli all the way from the upper to lower vertical meridian.

PRF size in hV4 is larger than in V3 and smaller than in LO-1

The pRF model fitting extends traveling-wave retinotopy by providing an estimate of the population receptive field size (Dumoulin & Wandell, 2008). Two robust trends found in the animal literature are that (i) receptive field size within a visual area increases with eccentricity (Hubel & Wiesel, 1974), and (ii) receptive field size for a given eccentricity increases along the posterior–anterior axis (Maunsell & Newsome, 1987).

Both trends are evident in the population receptive fields measured here (Figure 8). First, the pRF sizes in hV4 are larger than those in V1–V3 at all eccentricities and smaller than those in the LO and TO maps, especially at the higher eccentricities. There are no significant ventral–dorsal asymmetries in the pRF sizes in V2 or in V3. Second, in all 10 regions measured the pRF size increases as the mean eccentricity of the representation increases.

These pRF properties are generally in agreement with the separate measurements reported recently by Amano et al. (2009). However, the measured pRF sizes here are slightly larger, especially at the larger eccentricities (about 2 deg greater in most visual areas in the current measurements). This may be due to voxel size differences between the experiments (2.5 versus 1.5 mm isotropic voxels, a 4.6:1 ratio in volume). Additional factors limit the precision of the pRF size estimate, particularly at smaller eccentricities. The bar apertures are large relative to foveal receptive field sizes in early visual cortex. The large-bar stimulus is 28 deg in length and 3.5 deg in width, with 0.75 deg overlap between successive positions. Also, the TS artifact can affect measurements at the occipital pole in V1, V2, and V3 (Figure 10). Despite these limitations, the data clearly demonstrate that pRF size increases with eccentricity and across visual field maps, confirming the major trends observed in the animal literature. Additional measurements will be necessary to precisely quantify pRF size, particularly for voxels near the foveal representation.

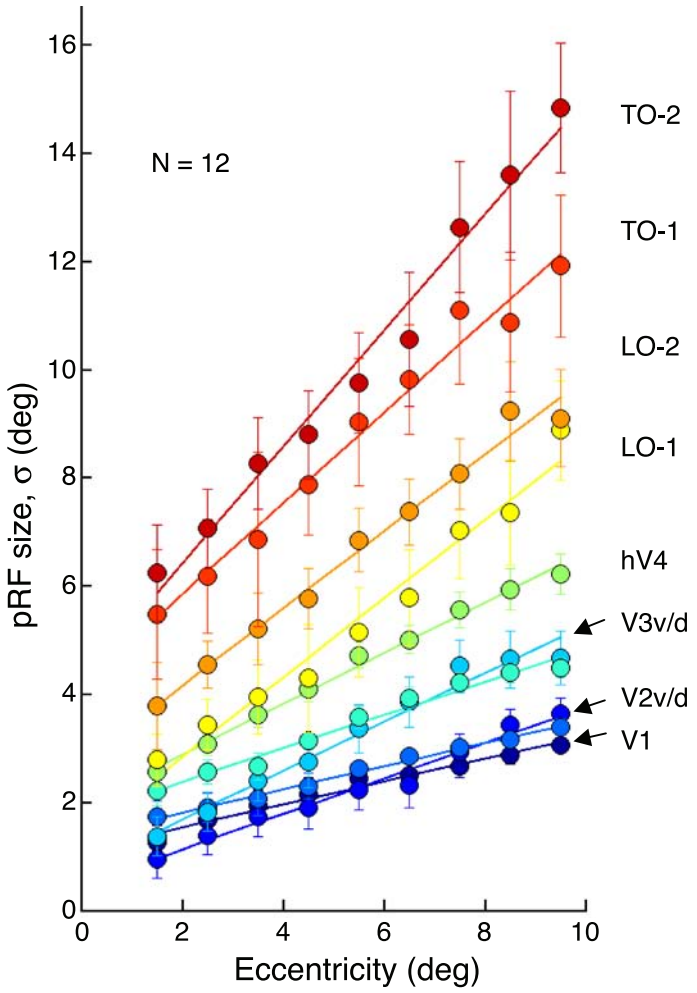

Figure 8. PRF size increases with eccentricity. In all visual field maps pRF size (std. dev. of the fitted Gaussian) increases with eccentricity. The hV4 pRF size at each eccentricity is intermediate between the smaller pRFs in V1–V3 and the larger pRFs in LO-1,2, and TO-1,2. PRF size measurements derived from measurements with the large (14°) stimulus. For each ROI in each hemispheres, pRF size was averaged across voxels in bins of 1° of eccentricity. Error bars show one standard error of the mean across 12 hemispheres. Arrows point to data for V1 (lower), V2d (middle), and V3d (upper).

Discussion

The purpose of our investigation was to measure the hV4 visual field coverage and evaluate the two models in Figure 1. The measurements were impeded by the TS

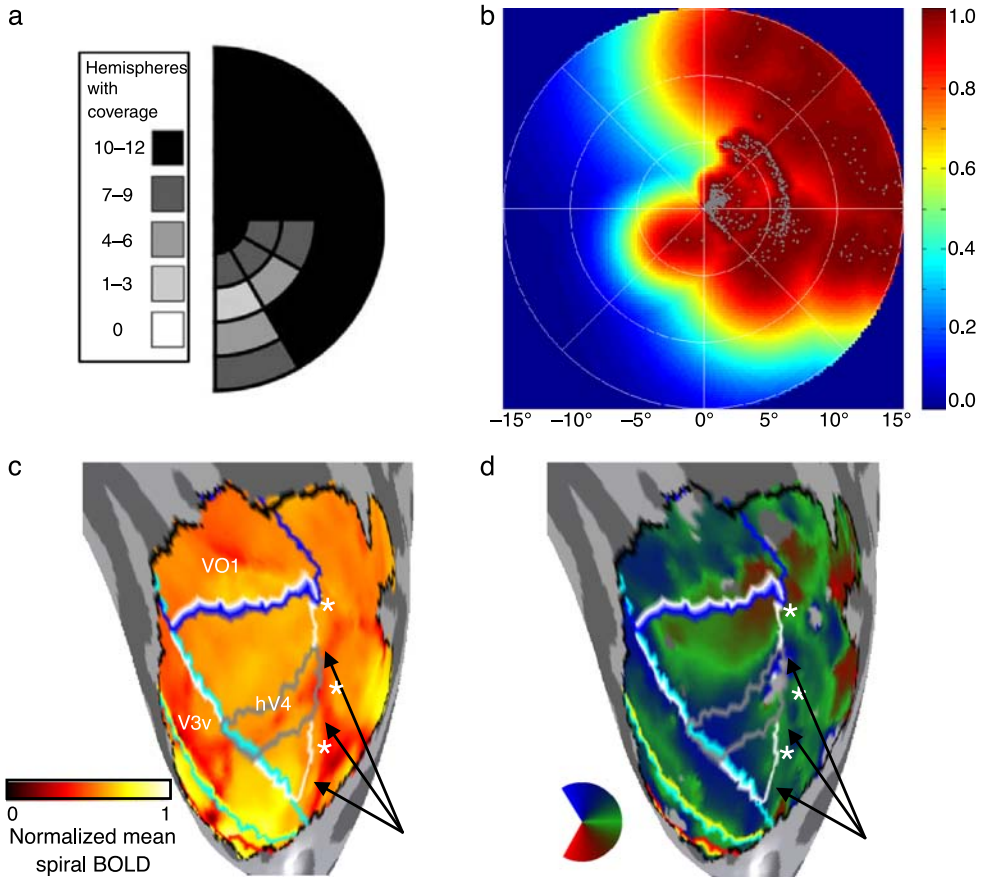

Figure 9. The TS artifact eclipses measurements from the lateral edge of hV4 in many subjects. (a) A summary of measurements from Hansen et al. (2007) shows that in many hemispheres ventral V4 fails to respond to sectors of the visual field near the lower vertical meridian. Data from the right hemispheres are flipped and pooled with data from the left hemispheres. (b) The pRF coverage in the left hemisphere (S5) does not extend to the lower vertical meridian. (c) The low mean BOLD signals show that the TS artifact (black arrows) runs along the lateral edge of hV4 (asterisks), interfering with the fMRI responses in this region. (d) The pRF model fits the responses in the TS artifact region with an upper field representation. Given our observation that the TS artifact regions often show counterphase responses to large field on–off stimuli, the pRF estimates in this region are also likely wrong; hence we cannot measure the full extent of the hV4 map in this subject.

artifact which frequently affects BOLD responses near the hV4 map. In light of this new observation, we revisit the interpretation of hV4 measurements in the literature.

Other groups investigating the hV4 map report significant variability across subjects. A summary of the Hansen et al. (Figure 9a) measurements shows that in only a few hemispheres the hV4 maps extend to the lower vertical meridian. Larsson and Heeger (2006), Arcaro, McMains, Singer, and Kastner (2009) and we confirm that in many hemispheres hV4 maps do not extend to the lower vertical meridian. For example, the hV4 visual field coverage data from the subject in Figure 6 (right image) does not reach the lower vertical meridian (Figure 9). The TS artifact distorts the fMRI signal and eclipses our view of the local cortical signals. When the TS is displaced from the lateral edge of hV4, eliminating the B_0 shift, the hV4 responses extend to the lower vertical meridian.

Human V4, color, and improbable areas

The idea of a unitary hV4 on the ventral surface originated with measurements of human color responses. Responses to color exchanges in human are nearly entirely confined to the ventral surface (Lueck et al., 1989; Zeki et al., 1991), while in macaque responses to the same color exchanges arise in both dorsal and ventral components of V4 (Wade, Augath, Logothetis, & Wandell, 2008). Additionally, human achromatopsia is caused by purely ventral lesions (Bouvier & Engel, 2006; Meadows, 1974; Zeki, 1990).

A further difficulty in defending a dorsal section of human V4 concerns the interpretation of the LO-1/2 maps, which were first described by Larsson and Heeger (2006) and subsequently confirmed by Amano et al. (2009). A dorsal V4 component would have to be subtracted from

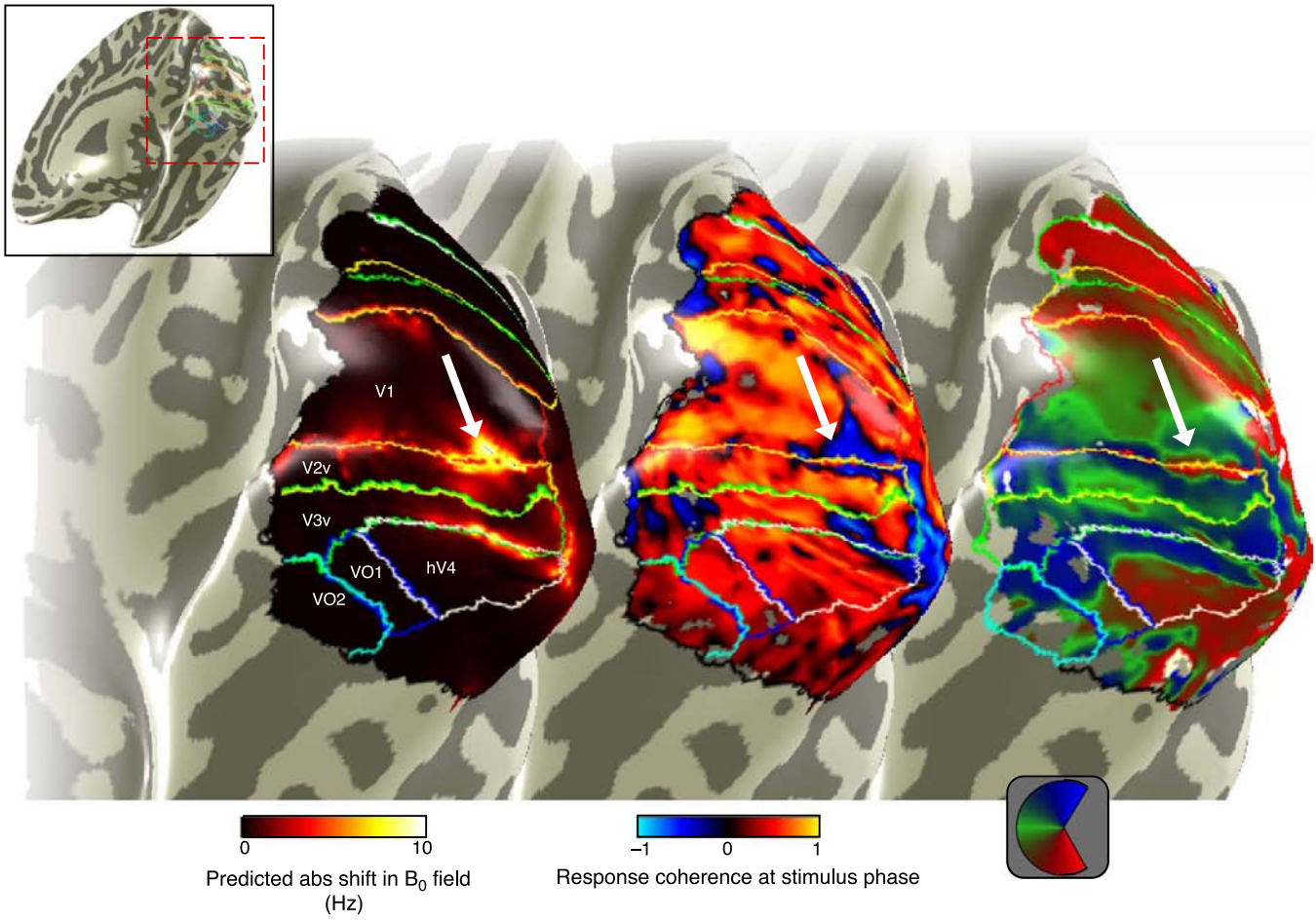

Figure 10. Position of the TS relative to foveal representations near the occipital pole. The three images show a posterior medial view of right occipital cortex with several visual field maps outlined (S3). (Left) The superimposed color map shows the predicted shift in the Larmor frequency caused by the B_0 field distortion from the nearby sinus. In this subject the predicted distortion is large along the ventral posterior border of V1/V2. (Middle) The color map shows the response coherence at the stimulus phase during large-field on–off scans. Responses in-phase with the stimulus are positive (hot colors); responses in counterphase are negative (cool colors). The locations with large predicted shifts in the Larmor frequency also show counterphase responses to the large-field stimulus. (Right) The angle map from the composite pRF model (14° and 3°) shows that these locations can have incorrect model solutions. For example, the ventral V1/V2 border is incorrectly assigned a lower field representation (red).

the LO-1 map, leaving an unexplained map fragment, or 'improbable area' (Zeki, 2003).

The TS affects measurements in V1–V3 at the occipital pole

The TS artifact distorts responses from a considerable amount of the cortical surface, often extending to the confluent V1–V3 foveal representation near the occipital pole. This region is notoriously difficult to measure using fMRI, though recent progress has been made by using high resolution functional imaging (Schira et al., 2009). As with the hV4 maps, the TS artifact at the occipital pole is expected based on calculations of the B_0 shift (Figure 10). The response to a large field on–off stimulation is in the wrong phase, making the artifact obvious. A more pernicious problem is that the TS artifact affects responses to more complex stimuli, such as the bars used for solving pRF models, leading to anomalous model fits. In both the on–off scans and the retinotopic scans, these anomalous responses sometimes exceed statistical threshold. There is significant inter-subject variability in the position of the artifact with respect to the V1–V3 maps.

The TS affects measurements of category selective cortical regions

The TS is near a large portion of VO cortex, and the corresponding artifact eclipses responses in category selective cortex. Cortical regions that respond more strongly to faces than other objects (Kanwisher et al., 1997) or to objects more than textures (Malach et al., 1995) can be near, or even overlapping, the TS artifact

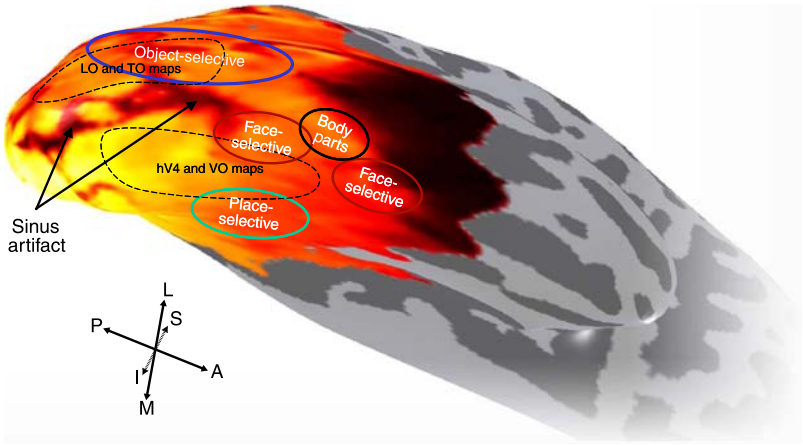

Figure 11. Position of the TS relative to category-selective regions in VO cortex. The color map measures the mean BOLD signal. The approximate locations of several category-selective regions are indicated by ellipses. In this right hemisphere (S5) the TS artifact lies between the ventral visual field maps and the lateral visual field maps; the artifact divides face and object selective regions. Category-selective regions were identified in independent localizer experiments by the Grill-Spector lab at Stanford University (Thanks to JMD Yoon and K. Weiner). Note that regions identified by category-specific localizers often overlap retinotopic maps (Sayres & Grill-Spector, 2008).

region. In the hemisphere shown in Figure 11 the right TS artifact falls between the ventral and dorsal maps (No man's land) and separates an object selective region from a face selective region. Generally, place selective regions such as the PPA (Epstein & Kanwisher, 1998) are remote from the TS artifact.

Conclusions

There has been much progress over the last twenty years in understanding the spatial organization, variability and response properties of the human visual field maps (Grill-Spector & Malach, 2004; Wandell et al., 2007). Much of this progress built on the important earlier work in animal models, particularly macaque (Felleman & Van Essen, 1991; Zeki, 1993). The much larger size of human visual cortex, and the need to efficiently wire the maps together (Van Essen, 1997), makes it likely that at some point the spatial organization of the human field maps diverges from those in macaque. In human and macaque, V4 may be a key gateway in transmitting essential information about form processing to ventral temporal areas (Desimone, Schein, Moran, & Ungerleider, 1985; Pasupathy & Connor, 2002). It is possible that pressure to shorten the wiring length between these ventral temporal regions and V4 caused hV4 to be located entirely on the ventral surface, closer to its primary projection zone. Hence, the fourth visual field map may be the first place where we can observe significant differences in how form processing is handled by these two visual systems.

Further advances in understanding hV4 and form processing can be achieved by improving fMRI methods for measuring signals in ventral occipital and temporal cortex. There are a number of significant artifacts that can arise when analyzing functional measurements and several of these are prominent in ventral cortex. Perhaps best known are the BOLD artifacts that are caused by moderately large pial veins (0.5–1 mm) adjacent to cortex and predominantly located in the sulci (Lee et al., 1995). Our efforts to understand the hV4 map have been limited by the very large dural veins (3–7 mm) that are closer to the gyri. The artifacts introduced by these two types of veins differ from one another. The pial veins carry blood oxygen from a large region of cortex, thus reducing the spatial specificity of the response and introducing significant noise into the signal (Duyn et al., 1995; Lee et al., 1995). Dagli et al. (1999) propose that some of this artifact can be eliminated by gating the stimulus presentation to the cardiac cycle. Olman et al. (2007) suggest that reducing voxel size can further improve the measurements because more voxels will escape the effects of the pial veins.

Here we analyze the distinct artifact that can be traced to the dural veins. These very large veins introduce a spatially localized shift in the local magnetic field; image reconstruction assumes a constant Larmor frequency and produces an incorrect result so that fMRI responses do not measure the cortical activity accurately. This artifact cannot be eliminated by averaging, cardiac-gating, or by shrinking the voxel size. It may be possible to reduce the artifact by using image reconstruction features that account for these spatially localized B_0 shifts (Man, Pauly, & Macovski, 1997).

Given the B_0 artifacts, we have taken the approach of using natural biological variability in the position of the dural sinuses to obtain estimates of the hV4 map. In taking this approach we find that there is a map on the ventral surface, hV4, whose responses span a hemifield. The population receptive field sizes of the responses from this map are larger than the sizes in V2, V3 and smaller than the sizes in LO-1/2 and TO-1/2. Continuing improvements in MR measurements,

including spatial resolution (Schira et al., 2009) and new reconstruction techniques (Man et al., 1997), will provide better data and a clearer view of the human visual field maps at millimeter or even sub-millimeter precision.

Appendix A

Expected artifact from the sinus

The shift in Larmor frequency (V_b) outside a vascular element due to the shift in the magnetic field is a function of several variables, including the vessel diameter (a), the distance from the vessel center (r), angle relative to the B_0 axis (theta), and angle in the cross-sectional plane of the vessel axis (phi).

$$V_b(r, \text{theta}, \text{phi}, a) = \text{Hct} * 2\text{pi} * \text{DeltaChi} * (1 - Y) * B_0^* \sin^2(\text{theta})(a/r)^2 * \cos(2 * \text{phi}). \quad \text{(A1)}$$

The other variables and the values we assumed for the schematic depicted in Figure 3b are B_0, the resonant frequency of water (1.28 * 10^8 Hz); Hct, blood hematocrit (0.4); DeltaChi, bulk susceptibility difference between fully oxygenated and fully deoxygenated blood (0.2 ppm); and Y, blood oxygenation level (0.6). The vessel diameter was assumed to be 7 mm, and the vessel axis relative to the B_0 field was either 0 deg (left), 45 deg (middle), or 90 deg (right). We depict the absolute value of the shift because positive and negative shifts are expected to have similar effects on the BOLD responses.

For the predicted B_0 maps in the cortex (Figures 3, 4, and 10) the diameter and angle relative to the B_0 field was estimated by fitting a series of cylinders (approximately one every 6 mm) along the skeleton of the transverse sinus, the superior sagittal sinus, and the straight sinus. The sinuses were labeled using an itk-Gray flood-fill tool on a venogram aligned to the high resolution T1-anatomy. For each voxel along the skeleton, there was a fitted cylinder yielding a radius and an angle relative to the magnetic field. The shift in the B_0 field was estimated by computing the shift field in the cross-sectional plane of each voxel along the skeleton. Because the skeleton curves, the cross-sectional planes intersecting nearby portions of the sinus often overlap producing more than one shift prediction for individual voxels. In these cases, we used the maximum prediction.

Appendix B

Response to large-field on–off stimulus as a function of predicted B_0 shift

We expect visual cortex to respond more to a large, moving contrast pattern than to mean luminance. Hence we expect that in the large-field on–off scans, most voxels in visual cortex will respond in phase with the contrast stimulus. This is in fact what we observe. However, for the subset of voxels in which the proximity to the sinus causes a shift in the B_0 field, the responses differ. For these voxels, particularly those with a predicted shift in Larmor frequency greater than 2 Hz, most voxels do not respond in phase to the stimulus (Figure B1). For many of these voxels, the response is in counterphase to the stimulus (upper plot, blue line) or significantly delayed

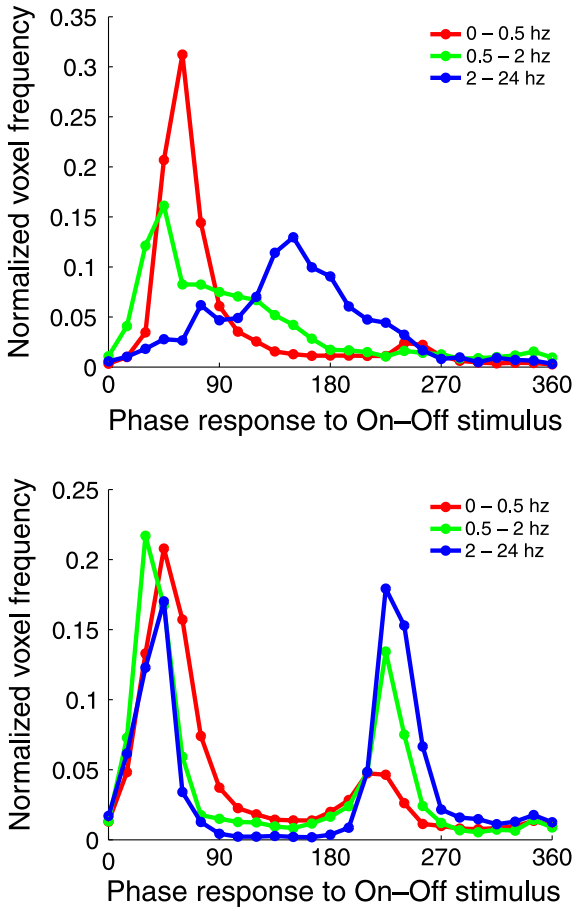

Figure B1. The TS artifact influences occipital cortex responses to large-field on–off stimuli. Voxels in right occipital cortex were binned by the size of the predicted shift in the Larmor frequency due to the B_0 distortion (S3, upper; S6, lower). When the predicted shift is low (<0.5 Hz; red), voxels generally respond in-phase with the stimulus (45°–60°, accounting for hemodynamic response function). When the predicted shift is large (>2 Hz; blue), many voxel responses are phase-delayed. For intermediate shifts (green), the distribution of response phases is intermediate. Only voxels with a coherence greater than 20% are included. Data come from the union of all the visual field maps (Figure 2) and "No man's land", the region between the ventral maps (hV4, VO-1/2) and the lateral maps (LO-1/2, TO-1/2). The on–off period was 24 s for S3 and 36 s for S6.

(lower plot, blue line). This pattern indicates that the B_0 distortion results in BOLD signals that do not measure the local cortical activity.

Appendix C

Mean maps and coverage, 12 hemispheres

The TS artifact often affects responses near hV4. Streaks of low mean spiral BOLD signals, usually running approximately along the poster-anterior axis, reveal the TS artifact (Figure C1). The streaks can appear as parallel bands when the TS artifact lies on the gyri on either side of a sulcus (e.g., subjects 1, 2, left hemispheres). The artifact and hV4 lateral edge frequently overlap in the left hemispheres (bottom row; e.g., subjects 1, 2, 5, and 6). In the right hemispheres, the TS artifact more often overlaps the posterior (foveal) part of hV4 than the lateral edge (e.g., subjects 1, 3, and 5). The visual field coverage in the right hemisphere tends to be greater than the left hemisphere.

The visual field coverage maps exclude the portion of cortex identified as being influenced by the TS. Had we included these regions, the coverage would be greater (adding voxels can only increase the coverage). However the large-field on–off responses in the TS artifact do not reflect the local cortical activity, so that we do not include data from these regions. The surface area of hV4, including the artifact regions, was 404 ± 179 mm^2 for the right hemispheres and 503 ± 163 mm^2 for the left hemispheres (means ± std).

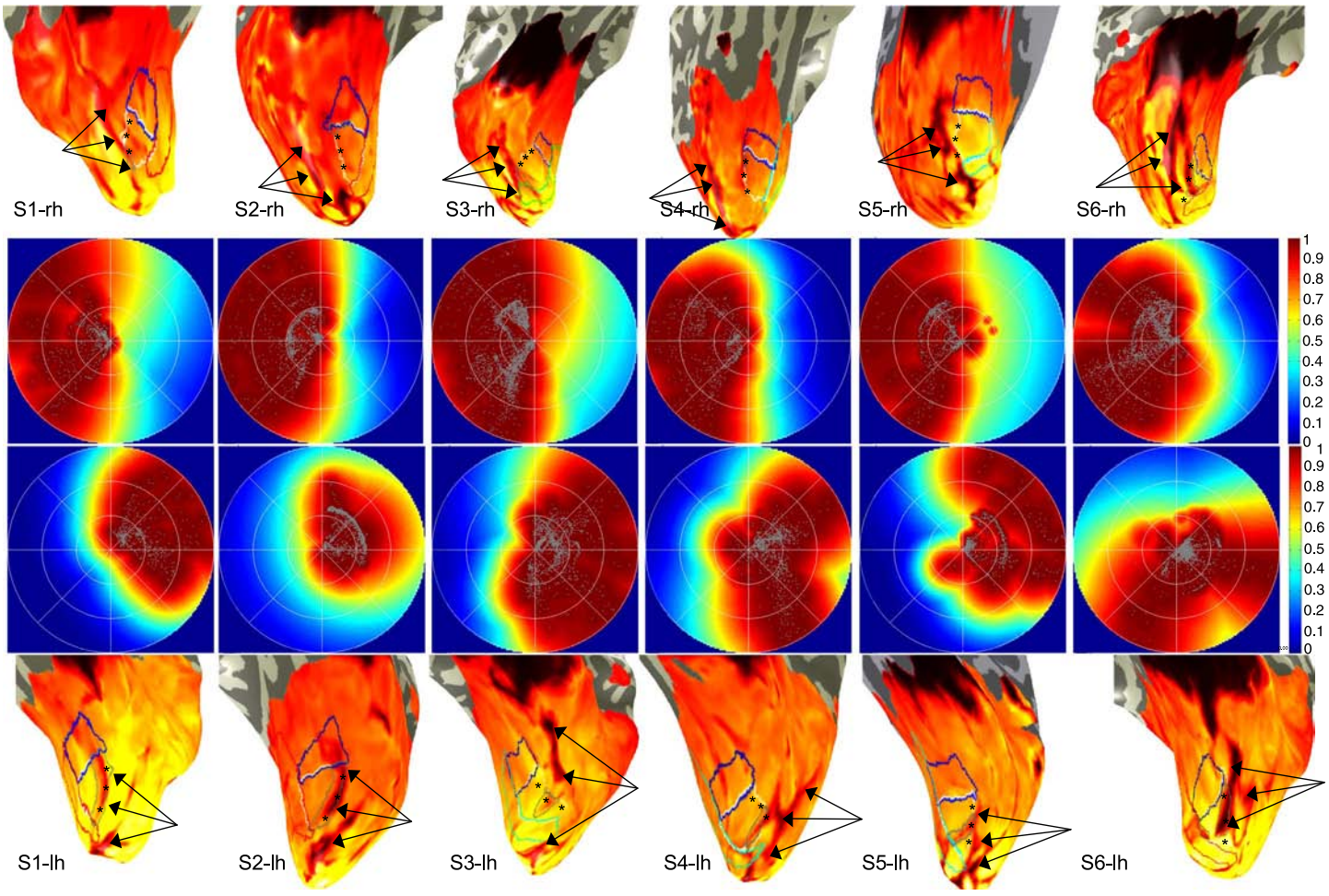

Figure C1. Mean BOLD maps and visual field coverage in 12 hemispheres. The ventral occipital cortex of both hemispheres in 6 subjects shows the mean BOLD signal (top and bottom panels. The location of the TS artifact is indicated with black arrows. The approximate hV4 boundaries are outlined in white and the lateral hV4 edge is denoted by asterisks. The gray outline marks regions where the TS artifact overlaps the presumed hV4 maps. Neighboring visual field maps are outlined (VO-1, blue; V3v, green or red). Plots showing the visual field coverage are either below (right hemispheres) or above (left hemispheres) the corresponding mesh.

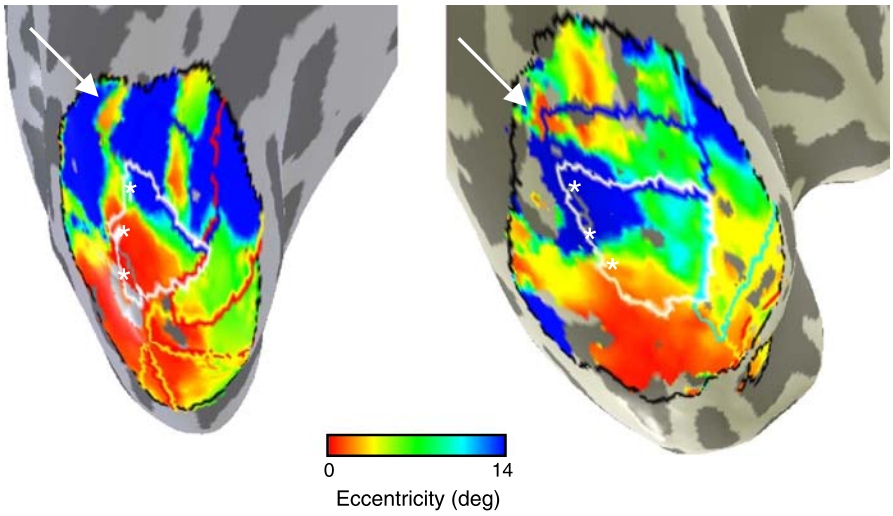

Figure C2. HV4 eccentricity maps in two hemispheres. S1 left; S4, right; both right hemispheres. White arrows indicate the expected location of the displaced foveal representation in VO-1/2.

hV4 eccentricity maps, 2 hemispheres

The eccentricity and angle maps of hV4, VO-1 and V3 come together in a three-corner arrangement that is difficult to measure. This region is particularly difficult to measure because the three maps appear to be oriented in different directions and yet they are in close proximity. The two maps in Figure C2 illustrate a likely hV4 eccentricity representation. The hV4 foveal representation is confluent with the V1–V2–V3 fovea near the occipital pole, and the hV4 peripheral representation is near the anterior edge of the map, near VO-1. The hV4 map does not extend as far anterior as the V1–V2–V3 maps, and its eccentricity representation increases more steeply along the posterior–anterior axis than the adjacent V3 ventral eccentricity representation.

In subject S4, but not S1, there is a clear view of the distinct foveal representation of the VO-1/2 maps, forming a separate visual field map cluster (Arcaro et al., 2009; Wandell, Brewer, & Dougherty, 2005). Like hV4, the VO cluster is frequently masked by the TS artifact. Further analyses that account for the artifact are needed to elucidate these maps.

Acknowledgments

This research was supported by National Institutes of Health Grants EY03164 (B.W.) and EY019224 (J.W.), and Grant-in-Aid for JSPS Fellows 20.11472 (HH). We thank Nicola Stikov for his insight about the B_0 distortions and Bob Dougherty for many helpful discussions. We also thank Semir Zeki for thoughtful comments on an earlier version of the manuscript.

Author contributions: Hiroshi Horiguchi and Rory Sayres contributed equally to this work.
Commercial relationships: none.
Corresponding author: Jonathan Winawer.
Email: winawer@stanford.edu.
Address: 450 Serra Mall, Stanford, CA 94305, USA.

Footnote

[1]Several components of the Methods adhere closely to those described in a prior publication from the same laboratory (Amano et al., 2009). Some text from the prior paper has been reproduced here with minor modifications in the sections Stimulus presentation (Visual field mapping stimuli); MR acquisition (Anatomical data, Functional data); and MR analysis (Pre-processing, PRF analysis, Visual field coverage).

References

Amano, K., Wandell, B. A., & Dumoulin, S. O. (2009). Visual field maps, population receptive field sizes, and visual field coverage in the human MT+ complex. *Journal of Neurophysiology, 102,* 2704–2718. [PubMed]

Arcaro, M. J., McMains, S. A., Singer, B. D., & Kastner, S. (2009). Retinotopic organization of human ventral visual cortex. *Journal of Neuroscience, 29,* 10638–10652. [PubMed]

Ashburner, J., & Friston, K. (2003). Rigid body registration. In R. S. J. Frackowiak, K. Friston, C. Frith, R. Dolan, C. J. Price, S. Zeki, & J. Ashburner (Eds.),

Human brain function (2nd ed., pp. xvi, 1144 p.). Amsterdam; Boston: Elsevier Academic Press.

Ben-Shachar, M., Dougherty, R. F., & Wandell, B. A. (2007). White matter pathways in reading. *Current Opinion Neurobiology, 17,* 258–270. [PubMed]

Bouvier, S. E., & Engel, S. A. (2006). Behavioral deficits and cortical damage loci in cerebral achromatopsia. *Cerebral Cortex, 16,* 183–191. [PubMed]

Boynton, G. M., Engel, S. A., Glover, G. H., & Heeger, D. J. (1996). Linear systems analysis of functional magnetic resonance imaging in human V1. *Journal of Neuroscience, 16,* 4207–4221. [PubMed] [Article]

Brainard, D. H. (1997). The Psychophysics Toolbox. *Spatial Vision, 10,* 433–436. [PubMed]

Brewer, A. A., Liu, J., Wade, A. R., & Wandell, B. A. (2005). Visual field maps and stimulus selectivity in human ventral occipital cortex. *Nature Neuroscience, 8,* 1102–1109. [PubMed]

Cohen, L., Dehaene, S., Naccache, L., Lehericy, S., Dehaene-Lambertz, G., Henaff, M. A., et al. (2000). The visual word form area: Spatial and temporal characterization of an initial stage of reading in normal subjects and posterior split-brain patients. *Brain, 123,* 291–307. [PubMed]

Dagli, M. S., Ingeholm, J. E., & Haxby, J. V. (1999). Localization of cardiac-induced signal change in fMRI. *Neuroimage, 9,* 407–415. [PubMed]

Desimone, R., Schein, S. J., Moran, J., & Ungerleider, L. G. (1985). Contour, color and shape analysis beyond the striate cortex. *Vision Research, 25,* 441–452. [PubMed]

DeYoe, E. A., Carman, G. J., Bandettini, P., Glickman, S., Wieser, J., Cox, R., et al. (1996). Mapping striate and extrastriate visual areas in human cerebral cortex. *Proceedings of the National Academy of Sciences of the United States of America, 93,* 2382–2386. [PubMed] [Article]

Dumoulin, S. O., & Wandell, B. A. (2008). Population receptive field estimates in human visual cortex. *Neuroimage, 39,* 647–660. [PubMed]

Duyn, J. H., Frank, J. A., Ramsey, N. R., Mattay, V. S., Sexton, R. H., Tallent, K. a., et al. (1995). Effects of large vessels in functional magnetic-resonance-imaging at 1.5 T. *International Journal of Imaging Systems and Technology, 6,* 245–252.

Epstein, R., & Kanwisher, N. (1998). A cortical representation of the local visual environment. *Nature, 392,* 598–601. [PubMed]

Felleman, D. J., & Van Essen, D. C. (1991). Distributed hierarchical processing in the primate cerebral cortex. *Cerebral Cortex, 1,* 1–47. [PubMed]

Friston, K. J., Fletcher, P., Josephs, O., Holmes, A., Rugg, M. D., & Turner, R. (1998). Event-related fMRI: Characterizing differential responses. *Neuroimage, 7,* 30–40. [PubMed]

Glover, G. H. (1999). Deconvolution of impulse response in event-related BOLD fMRI. *Neuroimage, 9,* 416–429. [PubMed]

Glover, G. H., & Lai, S. (1998). Self-navigated spiral fMRI: Interleaved versus single-shot. *Magnitude Reasoning Medical, 39,* 361–368. [PubMed]

Grill-Spector, K., Kushnir, T., Edelman, S., Itzchak, Y., & Malach, R. (1998). Cue-invariant activation in object-related areas of the human occipital lobe. *Neuron, 21,* 191–202. [PubMed]

Grill-Spector, K., & Malach, R. (2004). The human visual cortex. *Annual Review of Neuroscience, 27,* 649–677. [PubMed]

Hansen, K. A., Kay, K. N., & Gallant, J. L. (2007). Topographic organization in and near human visual area V4. *Journal of Neuroscience, 27,* 11896–11911. [PubMed] [Article]

Hubel, D. H., & Wiesel, T. N. (1974). Uniformity of monkey striate cortex: A parallel relationship between field size, scatter, and magnification factor. *Journal of Computer Neurology, 158,* 295–305.

Jancke, D., Erlhagen, W., Schoner, G., & Dinse, H. R. (2004). Shorter latencies for motion trajectories than for flashes in population responses of cat primary visual cortex. *The Journal of Physiology, 556,* 971–982.

Jezzard, P., & Ramsey, N. F. (2003). Functional MRI. In P. Tofts (Ed.), *Quantitative MRI of the brain: Measuring changes caused by disease* (pp. 413–454). Chichester, West Sussex; Hoboken, NJ: Wiley.

Kanwisher, N., McDermott, J., & Chun, M. M. (1997). The fusiform face area: A module in human extrastriate cortex specialized for face perception. *Journal of Neuroscience, 17,* 4302–4311. [PubMed] [Article]

Larsson, J., & Heeger, D. J. (2006). Two retinotopic visual areas in human lateral occipital cortex. *Journal of Neuroscience, 26,* 13128–13142. [PubMed] [Article]

Lee, A. T., Glover, G. H., & Meyer, C. H. (1995). Discrimination of large venous vessels in time-course spiral blood-oxygen-level-dependent magnetic-resonance functional neuroimaging. *Magnetic Resonance in Medicine, 33,* 745–754. [PubMed]

Lueck, C. J., Zeki, S., Friston, K. J., Deiber, M. P., Cope, P., Cunningham, V. J., et al. (1989). The colour centre in the cerebral cortex of man. *Nature, 340,* 386–389. [PubMed]

Maes, F., Collignon, A., Vandermeulen, D., Marchal, G., & Suetens, P. (1997). Multimodality image registra-

tion by maximization of mutual information. *IEEE Transactions on Medical Imaging, 16,* 187–198. [PubMed]

Malach, R., Reppas, J. B., Benson, R. R., Kwong, K. K., Jiang, H., Kennedy, W. A., et al. (1995). Object-related activity revealed by functional magnetic resonance imaging in human occipital cortex. *Proceedings of the National Academy of Sciences of the United States of America, 92,* 8135–8139. [PubMed] [Article]

Man, L. C., Pauly, J. M., & Macovski, A. (1997). Multifrequency interpolation for fast off-resonance correction. *Magnetic Resonance in Medicine, 37,* 785–792. [PubMed]

Martin, A., Haxby, J. V., Lalonde, F. M., Wiggs, C. L., & Ungerleider, L. G. (1995). Discrete cortical regions associated with knowledge of color and knowledge of action. *Science, 270,* 102–105. [PubMed]

Maunsell, J. H., & Newsome, W. T. (1987). Visual processing in monkey extrastriate cortex. *Annual Reviews of Neuroscience, 10,* 363–401.

McKeefry, D. J., & Zeki, S. (1997). The position and topography of the human colour centre as revealed by functional magnetic resonance imaging. *Brain, 120,* 2229–2242. [PubMed]

Meadows, J. C. (1974). Disturbed perception of colours associated with localized cerebral lesions. *Brain, 97,* 615–632. [PubMed]

Menon, R. S. (2002). Postacquisition suppression of large-vessel BOLD signals in high-resolution fMRI. *Magnetic Resonance in Medicine, 47,* 1–9. [PubMed]

Nestares, O., & Heeger, D. J. (2000). Robust multiresolution alignment of MRI brain volumes. *Magnetic Resonance in Medicine, 43,* 705–715. [PubMed]

Ogawa, S., Lee, T. M., Nayak, A. S., & Glynn, P. (1990). Oxygenation-sensitive contrast in magnetic resonance image of rodent brain at high magnetic fields. *Magnetic Resonance in Medicine, 14,* 68–78. [PubMed]

Olman, C. A., Inati, S., & Heeger, D. J. (2007). The effect of large veins on spatial localization with GE BOLD at 3 T: Displacement, not blurring. *Neuroimage, 34,* 1126–1135. [PubMed]

Pasupathy, A., & Connor, C. E. (2002). Population coding of shape in area V4. *Nature Neuroscience, 5,* 1332–1338. [PubMed]

Pelli, D. G. (1997). The VideoToolbox software for visual psychophysics: Transforming numbers into movies. *Spatial Vision, 10,* 437–442. [PubMed]

Press, W. A., Brewer, A. A., Dougherty, R. F., Wade, A. R., & Wandell, B. A. (2001). Visual areas and spatial summation in human visual cortex. *Vision Research, 41,* 1321–1332. [PubMed]

Sayres, R., & Grill-Spector, K. (2008). Relating retinotopic and object-selective responses in human lateral occipital cortex. *Journal of Neurophysiology, 100,* 249–267. [PubMed] [Article]

Schira, M. M., Tyler, C. W., Breakspear, M., & Spehar, B. (2009). The foveal confluence in human visual cortex. *Journal of Neuroscience, 29,* 9050–9058. [PubMed]

Teo, P. C., Sapiro, G., & Wandell, B. A. (1997). Creating connected representations of cortical gray matter for functional MRI visualization. *IEEE Transactions on Medical Imaging, 16,* 852–863. [PubMed]

Tootell, R. B., & Hadjikhani, N. (2001). Where is 'dorsal V4' in human visual cortex? Retinotopic, topographic and functional evidence. *Cerebral Cortex, 11,* 298–311. [PubMed] [Article]

Tootell, R. B., Mendola, J. D., Hadjikhani, N. K., Ledden, P. J., Liu, A. K., Reppas, J. B., et al. (1997). Functional analysis of V3A and related areas in human visual cortex. *Journal of Neuroscience, 17,* 7060–7078. [PubMed] [Article]

Tootell, R. B., Tsao, D., & Vanduffel, W. (2003). Neuroimaging weighs in: Humans meet macaques in "primate" visual cortex. *Journal of Neuroscience, 23,* 3981–3989. [PubMed] [Article]

Van Essen, D. C. (1997). A tension-based theory of morphogenesis and compact wiring in the central nervous system. *Nature, 385,* 313–318. [PubMed]

Victor, J. D., Purpura, K., Katz, E., & Mao, B. (1994). Population encoding of spatial frequency, orientation, and color in macaque V1. *Journal of Neurophysiology, 72,* 2151–2166. [PubMed]

Wade, A., Augath, M., Logothetis, N., & Wandell, B. (2008). fMRI measurements of color in macaque and human. *Journal of Vision, 8*(10):6, 1–19, http://journalofvision.org/content/8/10/6, doi:10.1167/8.10.6. [PubMed] [Article]

Wade, A., Brewer, A. A., Rieger, J. W., & Wandell, B. A. (2002). Functional measurements of human ventral occipital cortex: Retinotopy and colour. *Philosophical Transactions of the Royal Society of London B: Biological Sciences, 357,* 963–973. [PubMed] [Article]

Wandell, B., Brewer, A. A., & Dougherty, R. F. (2005). Visual field map clusters in human cortex. *Philosophical Transactions of the Royal Society of London, 360,* 693–707. [PubMed] [Article]

Wandell, B. A., Chial, S., & Backus, B. T. (2000). Visualization and measurement of the cortical surface. 739–752. [PubMed]

Wandell, B. A., Dumoulin, S. O., & Brewer, A. A. (2007). Visual field maps in human cortex. *Neuron, 56,* 366–383.

Worsley, K. J., Liao, C. H., Aston, J., Petre, V., Duncan, G. H., Morales, F., et al. (2002). A general statistical analysis for fMRI data. *Neuroimage, 15,* 1–15. [PubMed]

Yushkevich, P. A., Piven, J., Hazlett, H. C., Smith, R. G., Ho, S., Gee, J. C., et al. (2006). User-guided 3D active contour segmentation of anatomical structures: Significantly improved efficiency and reliability. *Neuroimage, 31,* 1116–1128. [PubMed]

Zeki, S. (1990). A century of cerebral achromatopsia. *Brain, 113,* 1721–1777. [PubMed]

Zeki, S. (1993). *A vision of the brain*. Oxford; Boston: Blackwell Scientific Publications.

Zeki, S. (2003). Improbable areas in the visual brain. *Trends in Neuroscience, 26,* 23–26. [PubMed]

Zeki, S., Watson, J. D., Lueck, C. J., Friston, K. J., Kennard, C., & Frackowiak, R. S. (1991). A direct demonstration of functional specialization in human visual cortex. *Journal of Neuroscience, 11,* 641–649. [PubMed] [Article]